



# Regulator of Calcineurin 1 helps coordinate whole-body metabolism and thermogenesis

David Rotter<sup>1,†</sup>, Heshan Peiris<sup>2,†</sup>, D Bennett Grinsfelder<sup>1</sup>, Alyce M Martin<sup>2</sup>, Jana Burchfield<sup>1</sup>, Valentina Parra<sup>3</sup>, Christi Hull<sup>1</sup>, Cyndi R Morales<sup>1</sup>, Claire F Jessup<sup>4</sup>, Dusan Matusica<sup>4</sup>, Brian W Parks<sup>5</sup>, Aldons J Lulis<sup>6</sup>, Ngoc Uyen Nhi Nguyen<sup>1</sup>, Misook Oh<sup>1,7</sup>, Israel Iyoke<sup>1</sup>, Tanvi Jakkampudi<sup>1</sup>, D Randy McMillan<sup>1,8</sup>, Hesham A Sadek<sup>1</sup>, Matthew J Watt<sup>9</sup>, Rana K Gupta<sup>10</sup>, Melanie A Pritchard<sup>11</sup>, Damien J Keating<sup>2,12,\*</sup>  & Beverly A Rothermel<sup>1,13,\*\*</sup> 

## Abstract

Increasing non-shivering thermogenesis (NST), which expends calories as heat rather than storing them as fat, is championed as an effective way to combat obesity and metabolic disease. Innate mechanisms constraining the capacity for NST present a fundamental limitation to this approach, yet are not well understood. Here, we provide evidence that Regulator of Calcineurin 1 (*RCAN1*), a feedback inhibitor of the calcium-activated protein phosphatase calcineurin (CN), acts to suppress two distinctly different mechanisms of non-shivering thermogenesis (NST): one involving the activation of UCP1 expression in white adipose tissue, the other mediated by sarcolipin (SLN) in skeletal muscle. UCP1 generates heat at the expense of reducing ATP production, whereas SLN increases ATP consumption to generate heat. Gene expression profiles demonstrate a high correlation between *Rcan1* expression and metabolic syndrome. On an evolutionary timescale, in the context of limited food resources, systemic suppression of prolonged NST by *RCAN1* might have been beneficial; however, in the face of caloric abundance, *RCAN1*-mediated suppression of these adaptive avenues of energy expenditure may now contribute to the growing epidemic of obesity.

**Keywords** adaptive thermogenesis; Down syndrome; obesity; *RCAN1*; sarcolipin

**Subject Category** Metabolism

DOI 10.15252/embr.201744706 | Received 26 June 2017 | Revised 12 September 2018 | Accepted 5 October 2018 | Published online 2 November 2018

EMBO Reports (2018) 19: e44706

## Introduction

Regulation of whole-body metabolism requires the integration of multiple organ systems that must respond appropriately to a diversity of internal and external stimuli. Disruption of this homeostatic balance underlies the growing epidemic in obesity, metabolic disease, and associated comorbidities. Enhancing innate thermogenic mechanisms that increase energy expenditure by dissipating it as heat has been championed as a promising approach for reducing storage of excess calories as fat. However, the body possesses multiple feedback mechanisms that on the whole work toward maintaining body weight [1]. Some thermogenic processes are constitutive in nature, contributing to an increase in resting energy expenditure (REE), while others are responsive, increasing energy expenditure only when activated. Heat generated by skeletal muscle, in animals at rest, is constitutive, whereas cold activation of the mitochondrial uncoupling protein 1 (UCP1) in brown adipose tissue (BAT) is an acute response. In cold-induced thermogenesis, increased adrenergic activity promotes lipolysis, releasing free fatty acids (FFA) that in turn activate UCP1 to release membrane potential as heat rather

1 Division of Cardiology, Department of Internal Medicine, University of Texas Southwestern Medical Center, Dallas, TX, USA

2 Department of Human Physiology and Centre for Neuroscience, Flinders University, Adelaide, SA, Australia

3 Faculty of Chemical and Pharmaceutical Sciences & Faculty of Medicine, Advanced Center for Chronic Diseases (ACCDiS) and Center for Exercise Metabolism and Cancer (CEMC), University of Chile, Santiago, Chile

4 Department of Anatomy and Histology and Centre for Neuroscience, Flinders University, Adelaide, SA, Australia

5 Department of Nutritional Sciences, University of Wisconsin-Madison, Madison, WI, USA

6 Division of Cardiology, Department of Medicine, University of California at Los Angeles, Los Angeles, CA, USA

7 Department of Chemistry, Pohang University of Science and Technology, Pohang, South Korea

8 Children's Medical Centre, Dallas, TX, USA

9 The Department of Physiology and Monash Biomedicine Discovery Institute, Metabolic Disease and Obesity Program, Monash University, Clayton, Vic., Australia

10 Touchstone Diabetes Center and Department of Internal Medicine, University of Texas Southwestern Medical Center, Dallas, TX, USA

11 Department of Biochemistry and Molecular Biology, Monash University, Melbourne, Vic., Australia

12 South Australian Health and Medical Research Institute (SAHMRI), Adelaide, SA, Australia

13 Department of Molecular Biology, University of Texas Southwestern Medical Centre, Dallas, TX, USA

\*Corresponding author. Tel: +61 8 82044282; Fax: +61 8 82045768; E-mail: damien.keating@flinders.edu.au

\*\*Corresponding author. Tel: +1 2146487428; Fax: +1 2146481450; E-mail: beverly.rothermel@utsouthwestern.edu

†These authors contributed equally to this work

than ATP production. UCP1 is most abundant in BAT, but under certain conditions, UCP1-positive (UCP1<sup>+</sup>) adipocytes appear in white adipose tissues (WAT) and have been termed “beige” or “brite” for brown-in-white adipocytes [2]. Prolonged cold exposure,  $\beta$ -adrenergic stimulation, or a high caloric diet can each increase “beiging” of WAT and primarily occurs in inguinal, subcutaneous WAT (sWAT) rather than in visceral WAT. Thus, adrenergic stimulation causes both an immediate adaptive thermogenic response by activating UCP1 and a long-term adaptive response by increasing UCP1 protein levels.

Although skeletal muscle in animals at rest has a relatively low metabolic rate, it comprises such a large percentage of body mass that in mammals it contributes 20–30% of REE [3]. Sarcoplipin (SLN) is a muscle-specific, sarcoplasmic reticulum (SR)-associated protein that when present increases heat production by uncoupling ATP hydrolysis from Ca<sup>2+</sup> transport by SERCA, the SR Ca<sup>2+</sup>-ATPase, thereby increasing ATP consumption at rest [4]. SLN is found in both skeletal muscle and heart. Mice lacking SLN are predisposed to diet-induced obesity, whereas skeletal muscle-specific overexpression provides protection [5–7]. Although mice lacking either *Ucp1* or *Slh* individually are able to survive acute cold exposure, loss of both genes severely compromises survival [8]. Thus, both UCP1 in adipose tissue and SLN in skeletal muscle are required for optimal thermogenesis under acute cold stress, although the molecular mechanisms used for thermogenesis by each are quite different; UCP1 reduces ATP production, whereas SLN increases ATP hydrolysis. The mechanisms providing coordination between these two systems are not fully understood. Here, we provide evidence that the gene, Regulator of Calcineurin 1 (*Rcan1*), exerts suppressive control over both mechanisms of thermogenesis, thereby contributing to systemic regulation of energy expenditure.

*Rcan1* (also known as *Dscr1/Mcip1*) is an endogenous inhibitor of the calcium-activated protein phosphatase, calcineurin [9,10]. Organ transplant patients receiving calcineurin inhibitors for immunosuppression are at increased risk for weight gain and new-onset diabetes [11,12]. In human genomewide association studies (GWAS), the *PPP3CA* locus, which encodes a catalytic subunit of calcineurin, is associated with both body mass index (BMI) and serum insulin levels [13]. Thus, both clinical and genetic data implicate calcineurin in metabolic regulation, although the underlying mechanisms are not known.

Calcineurin has many substrates including the transcription factor NFAT. A number of genes central to metabolic regulation have been identified as potential calcineurin/NFAT targets, including *insulin*, *Irs2*, and *resistin* [14–16]. Mice deficient for both *Nfatc2* and *Nfatc4* are resistant to diet-induced obesity [14]. In humans, polymorphisms in the *NFATc4* locus are associated with an increased risk for new-onset diabetes following organ transplant [17] and human GWAS studies show association of the *NFATc1*, *NFATc2*, and *NFATc3* loci with a variety of metabolic traits [13]. Calcineurin can also influence gene expression by activating cAMP response element binding protein (CREB)-regulated transcription co-activators (CRTCs). The CREB/CRTC axis is central to metabolic responses in a variety of tissues [18]. *CRTC1* polymorphisms influence BMI and fat mass in the general adult population [19], and a *CRTC2* polymorphism was identified as a risk factor for metabolic syndrome in transplant patients [20]. *CRTC3* variants are associated with adiposity [21] and cholesterol levels in adults [22]. Taken as a

whole, the range of genetic and phenotypic associations not only supports a model in which calcineurin-dependent transcription impacts body metabolism, but also suggests that multiple transcriptional mechanisms may be involved.

*Rcan1* is the best understood of the three mammalian *Rcan* genes [23] and generates two protein isoforms [24]. Both the RCAN1.1 and RCAN1.4 isoforms are potent calcineurin inhibitors; however, *Rcan1.4* expression is under the control of calcineurin/NFAT and thus forms an inhibitory feedback loop [25]. We previously showed that high glucose increases *Rcan1.1* transcription in pancreatic  $\beta$ -cells [26] and linked this to mitochondrial dysfunction and hypoinsulinemia in humans with T2D [27]. However, pancreatic function and growth appear to be normal in mice with the disruption of the gene encoding *Rcan1* (*Rcan1-KO*). Protein levels of both RCAN1 isoforms are high in a number of metabolically active tissues, including skeletal muscle, heart, and brain. Although there are currently no gene association studies in humans linking *RCAN1* to metabolic disorders, SNPs at the locus show a strong linkage to climate adaptation [28] and QTL studies in cattle show strong association between *Rcan1* and multiple adipose tissue traits [29], suggesting that *Rcan1* may have an as-yet-undefined role in mammalian adipocyte biology.

The *RCAN1* gene is located on human chromosome 21 and has been proposed as a key contributor to many of the phenotypes observed in individuals with Down syndrome (DS) [30]. Body weight regulation is a lifelong challenge in this population, which is also at greater risk for both type 1 and type 2 diabetes compared to weight- and age-matched peers [31]. We recently showed that mouse models of DS that were trisomic for the region containing the *Rcan1* locus are hyperglycemic, whereas those lacking this region are not [27], suggesting that one or more of the genes in this region are important to metabolism and glucose regulation. Here, we undertook a series of studies to better understand the role of RCAN1 in metabolic regulation. We show that *Rcan1-KO* mice are resistant to high-fat diet (HFD)-induced obesity because of an increase in whole-body metabolic rate when compared to wild-type (*WT*) controls. The mechanisms underlying the lean phenotype are multifaceted and include both increased expression of *Ucp1* in sWAT and increased expression of *Slh* in skeletal muscle. Our findings suggest that *Rcan1* helps to limit energy expenditure by acting directly as a brake on each of these adaptive, thermogenic processes. On an evolutionary timescale, in the context of limited food resources, these functions would be beneficial; however, in the face of current caloric abundance, *Rcan1*-mediated suppression of these adaptive avenues of energy expenditure may contribute to the growing epidemic in obesity.

## Results

### Mice deficient for *Rcan1* are resistant to diet-induced obesity

*WT* and *Rcan1-KO* mice were placed on a high-fat diet (HFD: 60% calories from fat) or maintained on normal rodent chow (NC) for 25 weeks. *WT* mice gained significantly more weight than the *Rcan1-KO* mice on either food source (Fig 1A and B). The difference in weight gain was not due to reduced food intake, as the calories consumed by the *KO* per gram of increase in body weight was greater than that of *WT* on either diet (Figs 1C and EV1A). The

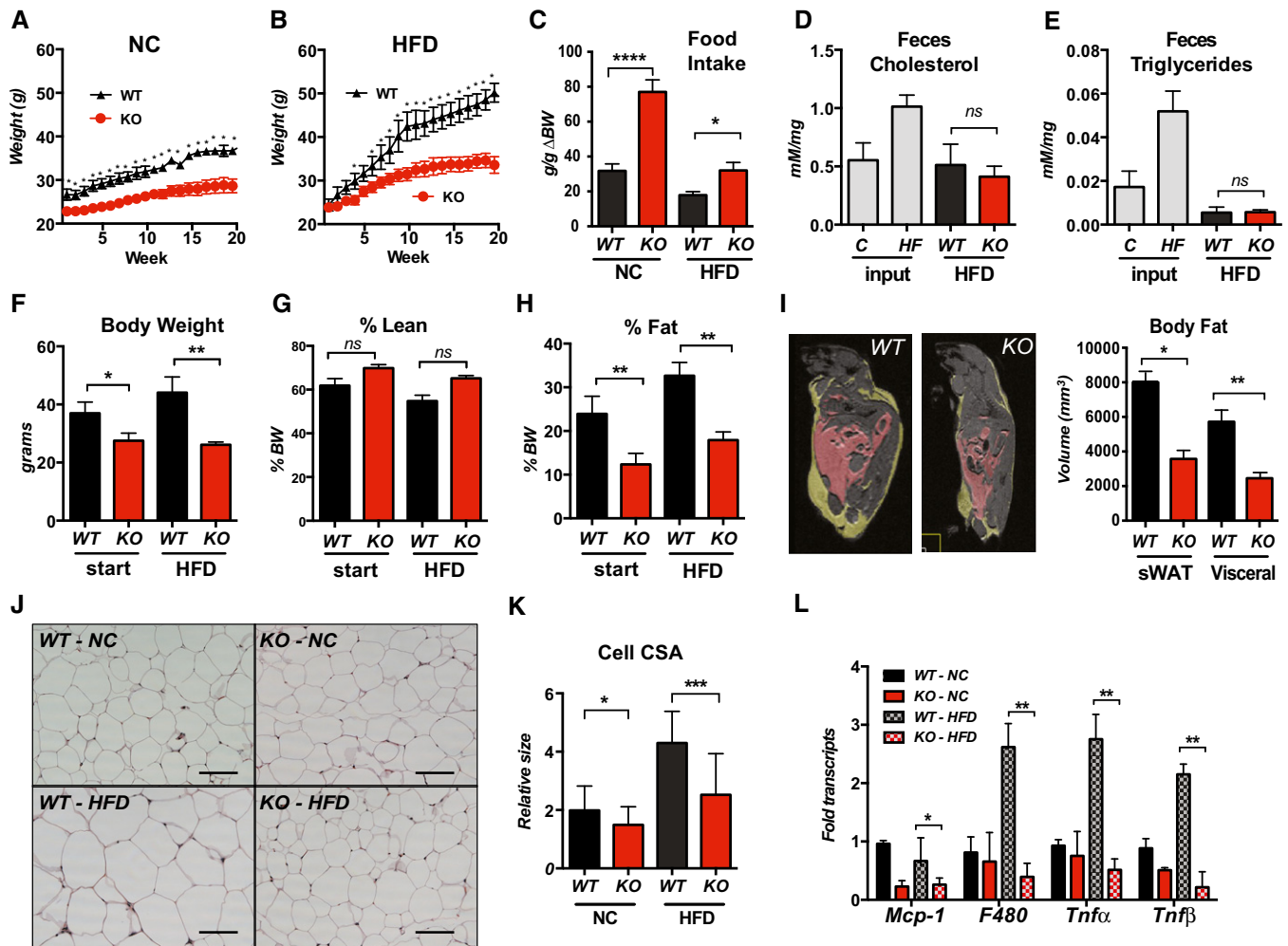


**Figure 1. *Rcan1*-KO mice are resistant to diet-induced obesity.**

A, B Body weights of WT and *Rcan1*-KO mice fed normal chow diet (NC) or a high-fat diet (HFD) for 20 weeks starting at 8–10 weeks of age (male,  $n = 15$  each).  
 C Food consumption per gram of body weight gained ( $g/g \Delta BW$ ) over the first 15 weeks on NC or HFD, starting at 8 weeks of age (male,  $n = 9$  each).  
 D, E Cholesterol and triglyceride remaining in the feces of WT and *Rcan1*-KO mice fed a HFD, measured as mMol per mg of feces (males,  $n = 4$  over 3 days). Cholesterol and triglyceride contents of NC and the HFD chow (input) were measured for comparison.  
 F–I MRI measures of total body weight, percentage lean mass, and percent fat mass prior to and after 6 weeks on the HFD (males,  $n = 5$ ). MRI image of WT and KO males following 8 weeks on a HFD. Yellow delineates visceral WAT. Pink delineates subcutaneous WAT. Quantification graphed on the right.  
 J Representative H&E staining of gWAT from WT and KO males after 25 weeks on NC or HFD. Scale bar = 100  $\mu m$ .  
 K Quantification of cross-sectional area (CSA) of adipocytes in (J) ( $n = 3$  animals, three images/each, 75–100 adipocytes). Scale bar = 100  $\mu m$ .  
 L Transcript levels for inflammatory markers monocyte chemoattractant protein-1 (*Mcp-1*), macrophage antigen *F4/80* (*F480*), tumor necrosis factor- $\alpha$  (*Tnf $\alpha$* ), and tumor necrosis factor- $\beta$  (*Tnf $\beta$* ) in gWAT of WT and KO after 25 weeks on NC or HFD (males,  $n = 4$ –5). Transcript levels were normalized to 18S.

Data information: Values shown are mean  $\pm$  SD except for graph in panel (I) where  $\pm$  SEM is indicated. \* $P < 0.05$ ; \*\* $P < 0.01$ ; \*\*\* $P < 0.001$ ; \*\*\*\* $P < 0.0001$  (two-way ANOVA with multiple comparisons, except for A and B, which used multiple  $t$ -tests).

amount of cholesterol and triglyceride remaining in the feces of KO and WT animals on the HFD were similar (Fig 1D and E); thus, the lean phenotype of the *Rcan1*-KO mice was not due to a defect in the ability to absorb dietary fat.

Nuclear magnetic resonance spectroscopy (NMR) analysis indicated that the primary difference between the two genotypes was body fat rather than lean mass (Fig 1F–H). This was verified by magnetic resonance imaging (MRI) showing significantly more fat deposition in WT animals than in KO after only 8 weeks on a HFD (Fig 1I). Upon histological examination, the average cross-sectional area of adipocytes was smaller in the gonadal fat pads (gWAT) of KO than in WT (Fig 1J

and K), suggesting a reduction in triglyceride storage at the level of individual adipocytes. Transcript levels for *Glut1* and *Glut4* were not significantly different in the adipose tissue depots of the KO compared to WT fed the HFD (Fig EV1B); thus, the smaller adipocyte size in the KO is not likely due to changes in glucose uptake.

Inflammation of visceral WAT stores typically precedes the onset of type 2 diabetes (T2D) and has been implicated in its onset [32]. Transcript levels for tumor necrosis factor- $\alpha$  (*Tnf $\alpha$* ), *Tnf $\beta$*  (*Tnf $\beta$* ), and the macrophage antigen *F4/80* were elevated in gWAT of HFD WT mice, whereas these signs of increased inflammation were absent in the gWAT of KO mice (Fig 1L). Transcripts for

monocyte chemoattractant protein-1 (*Mcp-1*) did not increase under HFD in our study but were lower in the *KO* regardless of diet.

Taken together, these data indicate that *Rcan1-KO* mice consume and absorb dietary fat at a rate similar to that of *WT* mice but store less of it as body fat. Furthermore, when on a HFD, the visceral fat stores of *KO* mice do not develop signs of inflammation and macrophage infiltration that are often indicative of a pre-diabetic state.

### *Rcan1-KO* mice maintain normal lipid handling and insulin sensitivity on a HFD

Oil Red O staining showed extensive liver steatosis in *WT* mice on HFD (Fig 2A). Lipid accumulation was significantly lower in

the livers of *KO* animals compared to *WT*, on either NC or HFD (Fig 2B). Transcript levels for genes involved in lipid handling and metabolism were elevated in the livers of *WT*, but not in the *KO*, including *stearoyl-coenzyme A desaturase (Scd1)*, *fatty acid transporter (CD36)*, *glycerol-3-phosphate acyltransferase (Gpat)*, and *carnitine palmitoyltransferase I (Cpt1)* (Fig 2C). Expression of genes involved in gluconeogenesis: *peroxisome proliferator-activated gamma (Pparg)* and *pyruvate dehydrogenase acetyl-transferase (Pdk4)* were likewise elevated in *WT* mice on HFD but not in *KO*. Conversely, there was a significant decrease in transcript levels for the facilitated glucose transporter (*Glut4*) in the livers of *WT* HFD mice but not *KO* (Fig 2C). There was no significant change in *peroxisome proliferator-activated receptor gamma coactivator 1*

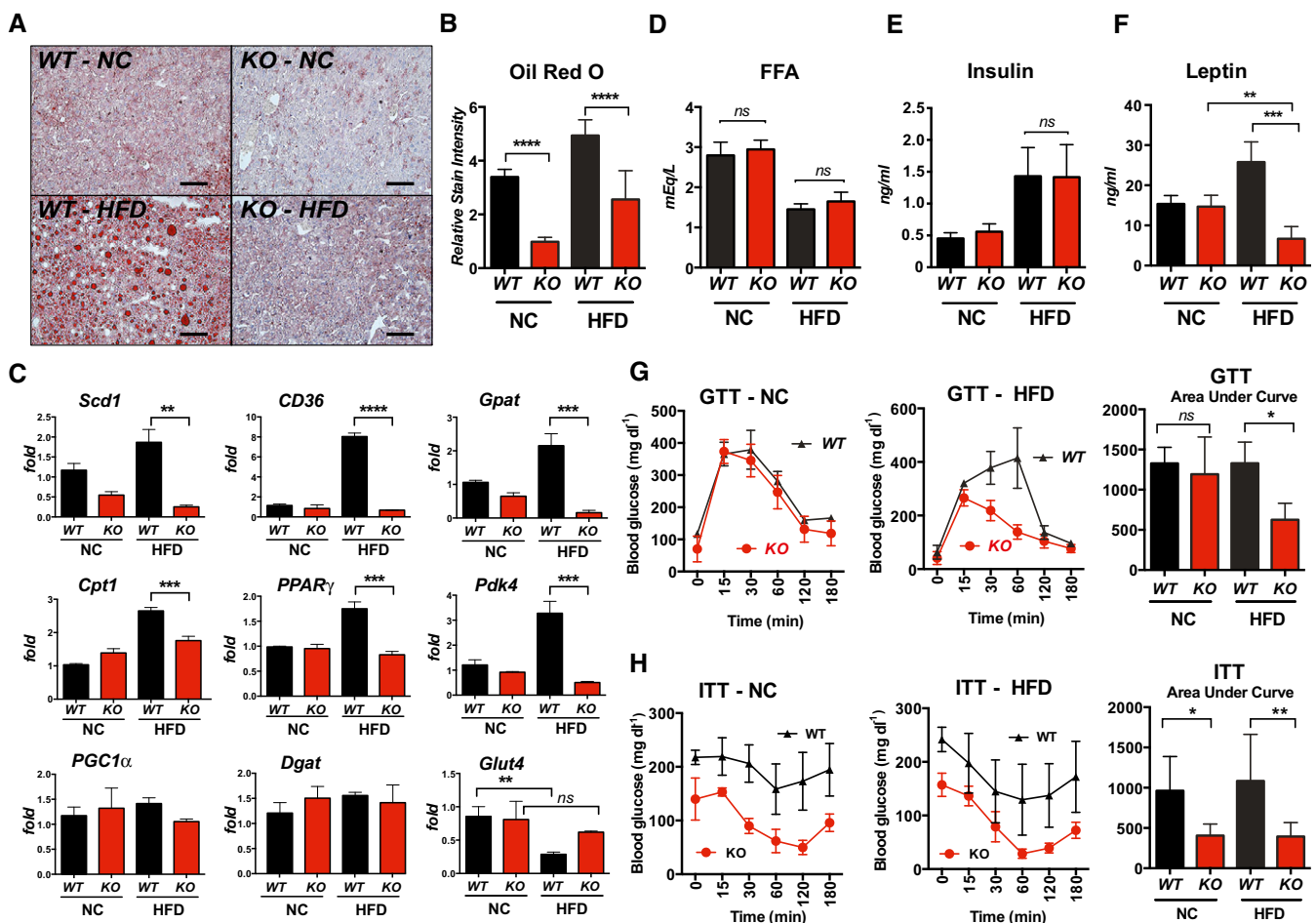


**Figure 2.** *Rcan1-KO* mice maintain normal lipid handling and insulin sensitivity on a HFD.

A, B Oil Red O staining of livers from *WT* and *KO* males after 25 weeks on NC or HFD, with quantification of relative stain intensity ( $n = 3$ , three images each). Scale bar = 100  $\mu\text{m}$ .

C Transcript levels for genes involved in lipid metabolism and gluconeogenesis in livers of *WT* and *KO* mice after 25 weeks on NC or HFD. *Stearoyl-Coenzyme A desaturase (Scd1)*, *fatty acid transporter (CD36)*, *glycerol-3-phosphate acyltransferase (Gpat)*, *carnitine palmitoyltransferase I (Cpt1)*, *peroxisome proliferator-activated gamma (PPAR $\gamma$ )*, *pyruvate dehydrogenase acetyl-transferase (Pdk4)*, *PPAR coactivator 1 alpha (PGC1 $\alpha$ )*, *diacylglycerol O-acyltransferase (Dgat)*, and *facilitated glucose transporter (Glut4)* (males,  $n = 4-5$ ). Transcript levels were normalized to 18S.

D-F Serum levels of free fatty acids (FAA), insulin, and leptin in *WT* and *KO* after 25 weeks on NC or HFD (males,  $n = 8-10$ ).

G, H Glucose tolerance test (GTT) and insulin tolerance test (ITT) after 25 weeks on NC or HFD. GTT was performed following an overnight fast, ITT following a 3-h fast (males,  $n = 6$ ).

Data information: Values shown are mean  $\pm$  SD. \* $P < 0.05$ ; \*\* $P < 0.01$ ; \*\*\* $P < 0.001$ ; \*\*\*\* $P < 0.0001$  (two-way ANOVA with multiple comparisons).



*alpha* (*Pgc1 $\alpha$* ) or *diacylglycerol O-acyltransferase* (*Dgat*) in either group.

Serum levels of nonesterified free fatty acids (FFA) were not significantly different in *KO* when compared to *WT* (Fig 2D). Both genotypes showed a similar decline in serum FFA when placed on a HFD, indicating reduced reliance on stored triglycerides. Insulin levels were similar in the two genotypes and increased comparably on the HFD (Fig 2E). An analysis of a wide panel of standard blood parameters also showed no significant difference between *KO* and *WT* (Fig EV1C). Finally, circulating levels of the adipokine leptin were the same in *WT* and *KO* animals on NC (Fig 2F), but significantly elevated only in the *WT* HFD animals, consistent with their pronounced increase in body fat mass.

Following an overnight fast, *WT* and *KO* animals on NC performed similarly in a glucose tolerance test (GTT) (Fig 2G). In contrast, in the animals maintained on a 60% HFD for 25 weeks, blood glucose levels remained elevated longer in the *WT* than in the *KO*, as evidenced by the significant difference in the area under the curves (Fig 2G). In an insulin tolerance test (ITT) following a 3-h fast, initial blood glucose levels in the *KO* were much lower than *WT* on either diet and remained lower throughout (Fig 2H). When normalized to starting levels, glucose uptake in the *KO* was likewise more pronounced (Fig EV1D). If animals were fasted for a longer period prior to the ITT assay, so that starting blood glucose levels were comparable in the *WT* and *KO*, the *KO* mice frequently died of hypoglycemic shock when injected with insulin, particularly those on a high-fat diet. To evaluate how quickly differences in glucose handling were manifest, we tracked a separate cohort of animals and found significant differences in glucose uptake between the two genotypes by only 8 weeks on the HFD (Fig EV1F). Similar differences in weight gain were observed on a 35% fat diet (Fig EV2A). Furthermore, when maintained on normal chow for a year, *KO* mice had improved glucose tolerance and insulin sensitivity compared to *WT* (Fig EV2B). Thus, the *KO* mice were resistant to age-dependent declines in glucose metabolism and handling.

### Whole-body metabolism is elevated in mice lacking *Rcan1*

Although we observed dramatic phenotypic differences between *WT* and *KO* mice on a HFD, these differences were primarily those one would expect to find when comparing an obese mouse with a lean one. As such, they provide limited insight into the underlying processes being influenced by *Rcan1*. Therefore, we focused our analysis on identifying metabolic differences between 12-week-old *KO* and *WT* mice on normal chow. Whole-body rates of both oxygen consumption ( $VO_2$ ) and carbon dioxide production ( $VCO_2$ ) were significantly elevated in *KO* mice compared to *WT*, indicating an increased rate of metabolism (Fig 3A and B). However, there was no difference in the respiratory exchange ratio (RER) (Fig 3C), demonstrating similar substrate preferences and normal circadian shifts between glucose and fatty acid oxidation. Importantly, there was no significant difference in the physical activity between the two genotypes (Fig 3D); thus, the elevated metabolic rate of the *KO* was not due to a change in physical activity.

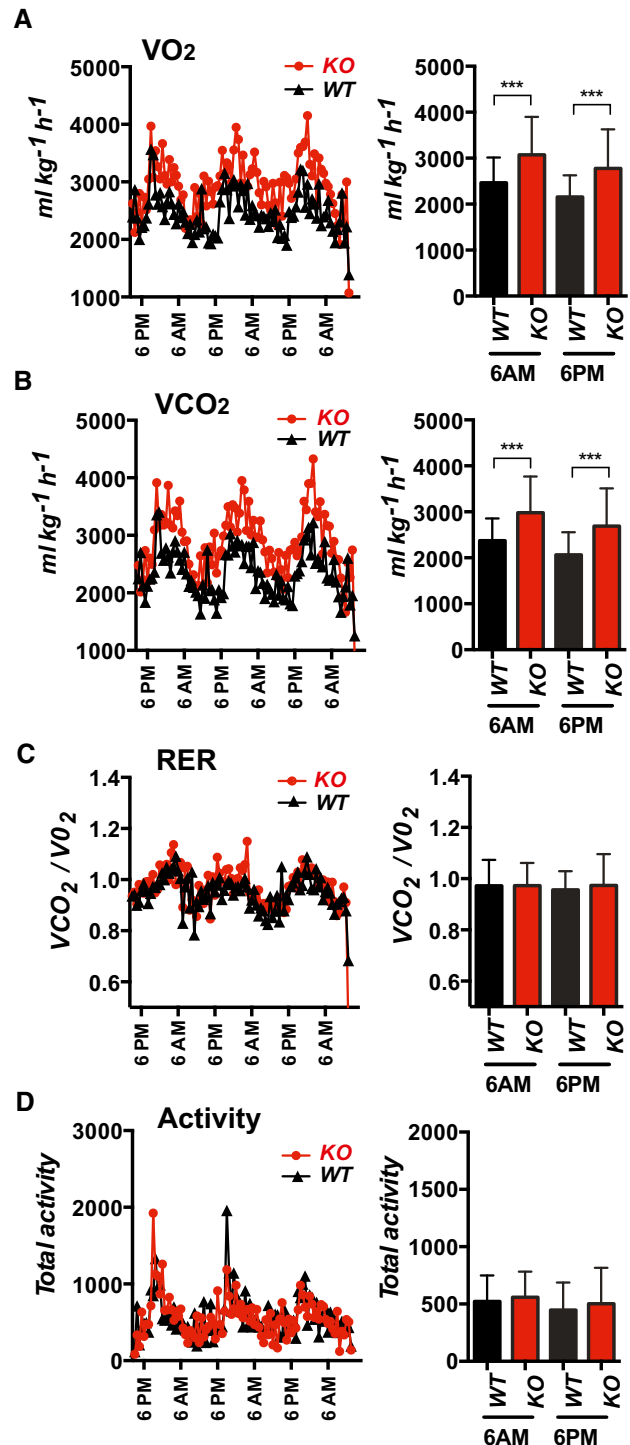


**Figure 3. Whole-body metabolism is elevated in the *Rcan1*-*KO*.**

A–D Oxygen consumption ( $VO_2$ ), carbon dioxide production ( $VCO_2$ ), respiratory exchange ratio  $VCO_2/VO_2$  (RER), and physical activity of 10- to 12-week-old *WT* and *KO* mice on normal chow were measured using the CLAM metabolic cage system (males,  $n = 6$ ). Bar graphs show the average value of metabolic measurements made within the 60 min flanking 6 AM or 6 PM. Values shown are average  $\pm$  SD. \*\*\* $P < 0.001$  (two-way ANOVA with multiple comparisons).

### Depletion of Rcan1 reduces lipid accumulation in differentiated 3T3-L1 adipocytes

RCAN1.1 protein could be detected by Western blot in extracts of BAT, sWAT, and gWAT from both male and female animals, although in lower abundance than in striated muscle or brain (Fig EV3A and B). To test for RCAN1 adipocyte-autonomous functions, we used 3T3-L1 preadipocytes. Changes in transcript levels of both *Rcan1.1* and *Rcan1.4* were quantified by RT-PCR following treatment with MDI (medium containing 3-isobutyl-1-methyl-xanthine, dexamethasone, and insulin) to induce differentiation (Fig 4A). *Rcan1.1* transcript levels remained relatively constant throughout the time course, whereas *Rcan1.4*, whose expression is under the control of calcineurin/NFAT [25], was more dynamic, suggesting a rapid transient activation of calcineurin in response to MDI, followed by a more modest, gradual rise later in differentiation. siRNAs targeting each of the isoforms were used to deplete *Rcan1* transcripts prior to differentiation. Knockdown (KD) was efficient and sustained over a 10-days course of differentiation (Fig 4B). Lipid accumulation was markedly reduced in the *Rcan1.1* KD cultures compared to controls as assessed by Oil Red O (Fig 4C). The effect of the *Rcan1.4* KD on lipid accumulation was much less pronounced, but still evident. Depletion of *Rcan1* did not prevent or delay adipocyte differentiation as all treatment groups began releasing adiponectin into the culture media at a similar time (Fig 4D). Transcript levels for *Pgc1 $\alpha$* , which plays a central role in the activation of the brown and beige adipocyte program [33] increased over the 10-days course of differentiation in all cultures; however, expression was higher in the *Rcan1.1* KD adipocytes at all time points (Fig 4E). *Ucp1* transcript levels were below detection.

### Adrenergic stimulation of Pgc1 and Ucp1 expression is enhanced in subcutaneous adipocytes depleted of Rcan1

The increase in *Pgc1 $\alpha$*  expression and decrease in lipid accumulation observed in *Rcan1*-depleted 3T3-L1 adipocytes, coupled with the lean phenotype of the *Rcan1*-KO mice, suggest that *Rcan1* may act to suppress differentiation of adipocytes toward a brown or beige phenotype. To study this in cells capable of activating *Ucp1*

expression, we established an immortalized preadipocyte cell line, *Ing-svf*, using stromal vascular cells (SVCs) isolated from sWAT of WT C57BL/6 mice. *Ing-svf* cultures were transfected with control or *Rcan1*-targeted siRNA (targets both *Rcan1* isoforms), then differentiated for 10 days. Similar to the *Rcan1*-depleted 3T3-L1 adipocytes, lipid droplet size appeared smaller in the *Rcan1*-depleted *Ing-svf* adipocytes than in the control siRNA-treated cultures (Fig 4F). Importantly, upon differentiation, the *Ing-svf* cultures depleted for *Rcan1* showed elevated expression of the beta-3 adrenergic receptor, *Adrb3*, which is required for cold induction of *Ucp1* in sWAT [2] (Fig 4G). Following adrenergic stimulation with isoproterenol (ISO), transcript levels for *Pgc1 $\alpha$* , *Ucp1*, and type II deiodinase (*Dio2*) were higher in *Rcan1*-depleted cultures than in the control siRNA cells, suggesting an increased being response in the absence of *Rcan1*. To determine whether these differences were manifest in the adipocyte progenitors of the *Rcan1*-KO mice, fluorescence-activated cell sorting (FACS) was used to isolate platelet-derived growth factor receptor alpha-positive and lineage-negative (PDGFR $\alpha$ <sup>+</sup>/Lin<sup>-</sup>) SVCs from the sWAT of WT and *Rcan1*-KO mice. When maintained in growth media, there was no significant difference in expression of a wide panel of genes related to adipocyte differentiation and metabolic phenotype (Fig 4H). However, following differentiation with MDI, expression of a number of these genes, including *Pgc1 $\alpha$* , *Ppar $\gamma$ 1*, and *Ppar $\gamma$ 2*, was higher in the cultures derived from the *Rcan1*-KO than in those derived from WT (Fig 4I). Taken together, these studies suggest that *Rcan1* has an adipocyte-autonomous inhibitory effect on differentiation toward a UCP1<sup>+</sup>, thermogenic beige/brown phenotype.

### Cold-induced “being” of subcutaneous WAT is enhanced in the Rcan1 KO

To compare the cold-induced being response of KO with that of WT, animals were housed for 5 days in a 6°C environment or maintained under normal vivarium temperatures (RT = 24°C). The morphology of the fat pad and extent of UCP1<sup>+</sup> staining were similar in the WT and KO animals housed at RT. Both genotypes showed a mosaic of uni- and multi-locular adipocytes with patchy regions of low-intensity UCP1<sup>+</sup> staining (Fig 5A). Following 5 days of cold

**Figure 4. Depletion of Rcan1 reduces adipocyte lipid accumulation in vitro.**

- A Transcript levels for *Rcan1.1* and *Rcan1.4* during differentiation of 3T3-L1 adipocytes, measured at 0, 1, 2, 3, 4, 6, and 24 h following the addition of MDI as well as at 3, 7, and 10 days as indicated ( $n = 3$ ). \* $P < 0.05$ ; \*\* $P < 0.01$  (unpaired Student's  $t$ -test versus 0 time point).
- B Western blot for RCAN1.1, RCAN1.4, and tubulin (TUB) in whole-cell extracts of 3T3-L1 adipocytes transfected with a control siRNA or ones targeting either *Rcan1.4* or *Rcan1.1* (20  $\mu$ g per lane).
- C Representative images of 3T3-L1 adipocytes transfected with the indicated siRNAs prior to differentiation and stained with Oil Red O on day 10. Scale bar = 100  $\mu$ m.
- D Western blot for adiponectin (ADPOQ) released into the media during differentiation by 3T3-L1 adipocytes transfected with the indicated siRNAs. Ponceau-stained image provides loading control.
- E Transcript levels for *Pgc1- $\alpha$*  in 3T3-L1 adipocytes transfected with the indicated siRNAs and assayed over 10 days of differentiation ( $n = 3$ ).
- F Representative bright-field images showing lipid accumulation at 10 days of differentiation of *Ing-svf* cells treated with the indicated siRNA. Scale bar = 50  $\mu$ m.
- G Transcript levels for *Adrenoceptor beta 3* (*Adrb3*), *uncoupling protein 1* (*Ucp1*), *PPAR $\gamma$  coactivator 1 alpha* (*PGC1 $\alpha$* ), and *deiodinase type II* (*Dio2*) in *Ing-svf* cultures transfected with control siRNA (C) or one targeting *Rcan1* (KD) then maintained in growth media (G), or differentiated for 10 days (D) with and without the addition of 100 mM isoproterenol for 6 h prior to harvesting (D+ISO) ( $n = 2$  in triplicate). \* $P < 0.05$ ; \*\* $P < 0.01$  (two-way ANOVA with multiple comparisons).
- H, I Transcript levels for the indicated panel of genes relevant to adipocyte differentiation in platelet-derived growth factor receptor alpha-positive (PDGFR $\alpha$ <sup>+</sup>) and lineage-negative (Lin<sup>-</sup>) stromal vascular cells isolated by FACS analysis sorting from sWAT of WT (black bars) and KO (red bars). In (H), isolated cells were maintained in growth media. In (I), cultures were treated with MDI then differentiated for 10 days. \* $P < 0.05$ ; \*\* $P < 0.01$  (unpaired Student's  $t$ -test, WT versus KO time point) ( $n = 3$ ).

Data information: Transcript levels were normalized to 18S. All values shown are mean  $\pm$  SD.

exposure, the increase in UCP1<sup>+</sup> signal was more pronounced in the KO animals. In animals maintained at RT, *Pgc1α* and *Ucp1* transcript levels were similar in WT and KO, although significantly higher in the sWAT of males than in females (Fig 5B). Following 24-h exposure to 4°C, cold induction of *Pgc1α* and *Ucp1* in sWAT of females was significantly greater in KO than WT (Fig 5B). In males, the cold-induced response trended toward higher in KO, but did not reach statistical significance. Diet-induced beiging of sWAT in response to a prolonged HFD was also greater in the KO, as evidenced by higher transcript levels for *Pgc1α*, *Ucp1*, and *Adrb3* (Fig 5C). Thus, animals deficient for *Rcan1* showed enhanced activation of adaptive thermogenesis in sWAT in response to either

temperature or diet. In contrast, there was no significant difference in the transcript levels for several genes involved in BAT specification (*pRB1*, *Zfp423*, and *Prdm16*) in the sWAT of KO compared to WT fed a HFD (Fig 5C). Taken together, these data suggest that *Rcan1* suppresses both diet- and cold-induced adaptive thermogenesis of WAT, through a mechanism involving the *Pgc1α/Ucp1* axis.

#### Rcan1-dependent control is specific for the *Pgc1α-1b* transcript during cold-induced beiging of sWAT

*Pgc1α* is required for transcriptional activation of cold-induced adaptive thermogenesis [33]. The *Pgc1α* gene produces multiple

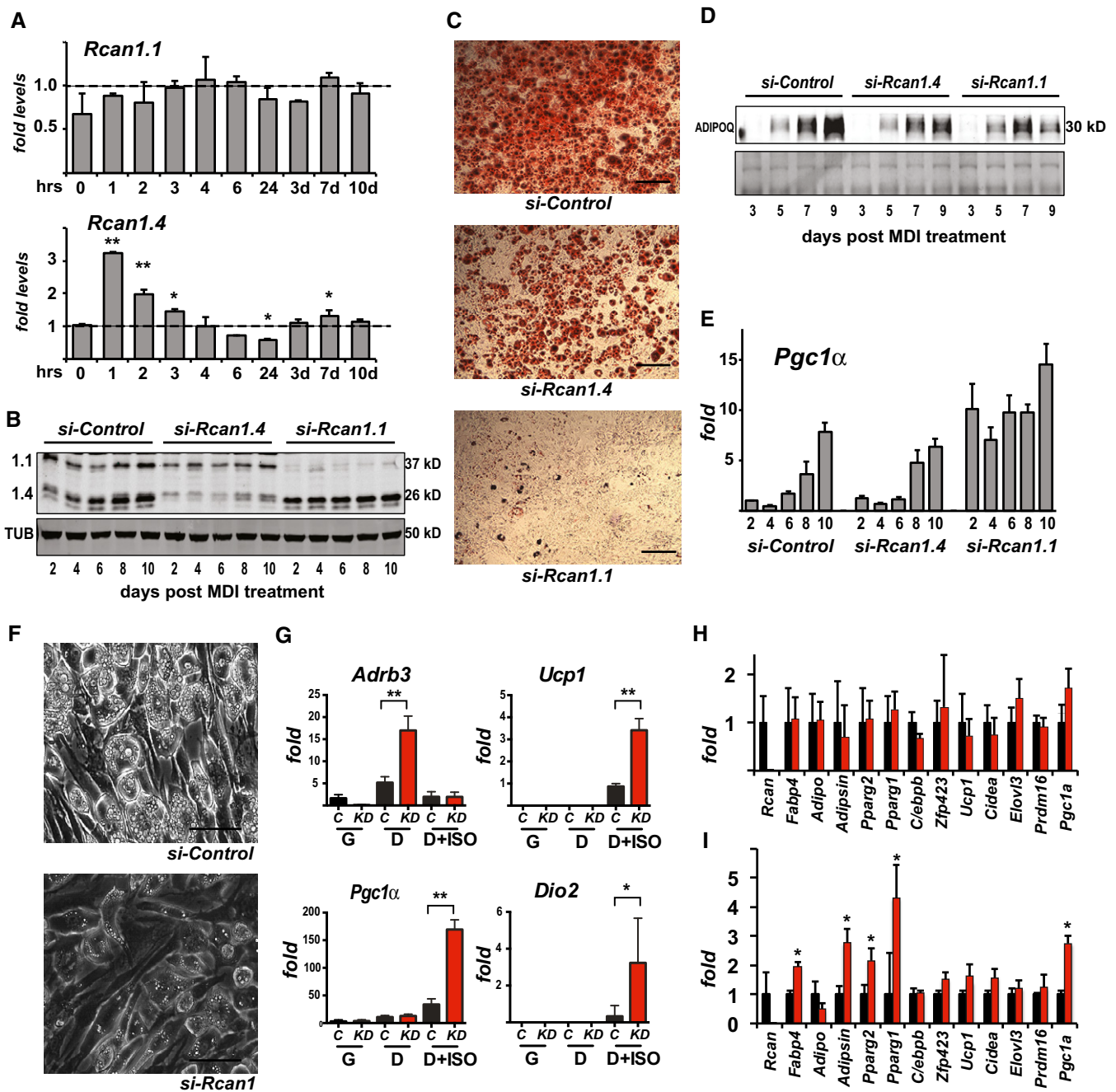
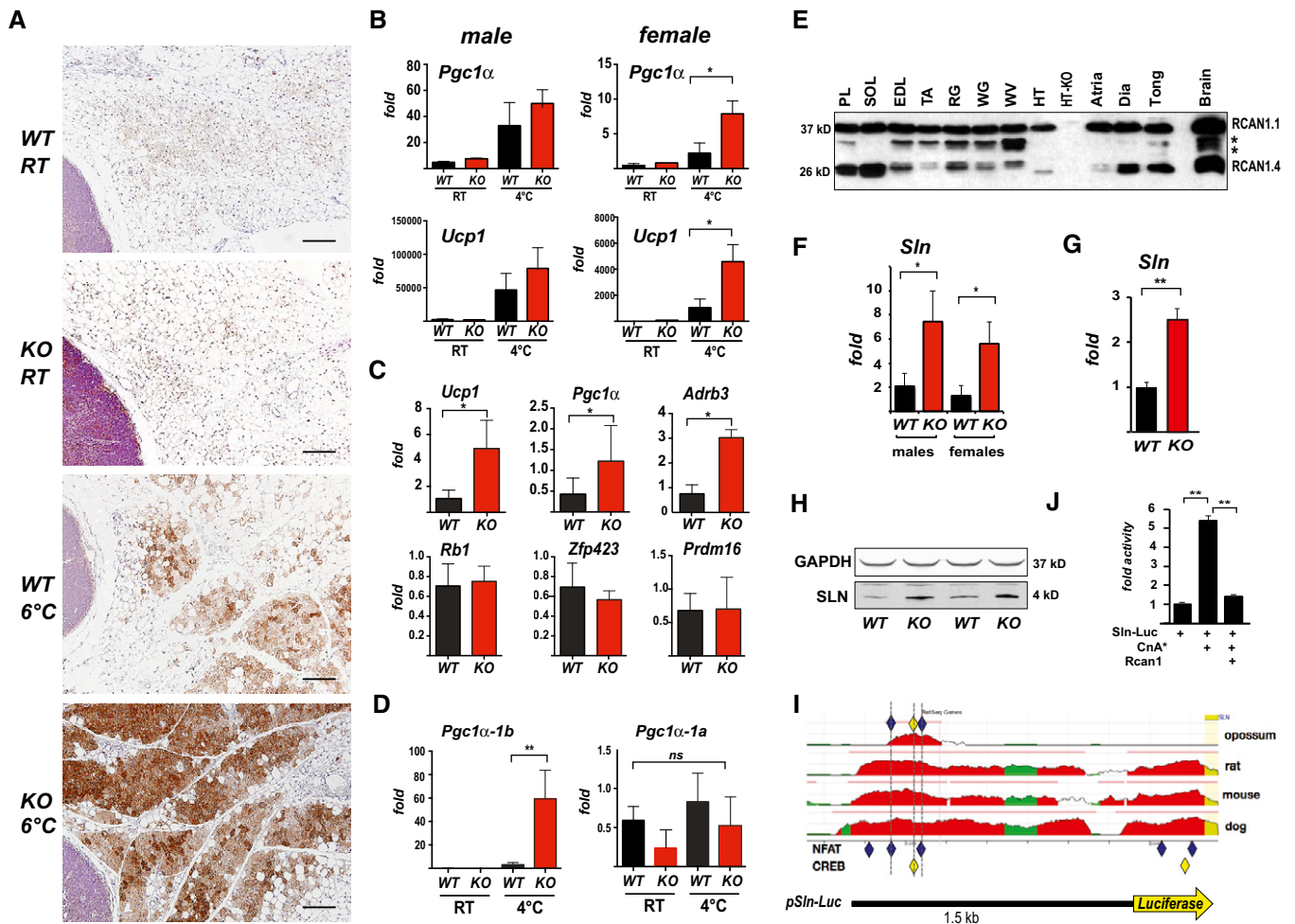


Figure 4.





**Figure 5. Rcan1-KO mice show enhanced beiging of adipocytes in sWAT and elevated expression of SLN skeletal muscle.**

**A** Representative H&E histological sections of sWAT from WT and KO mice probed with anti-UCP1 antibodies. Mice were either maintained at 24°C (RT) or housed at 6°C for 5 days. Scale bar = 200 μm.

**B** Transcript levels of *Pgc1α* and *Ucp1* in sWAT of male and female WT and KO mice after 24 h at RT or 4°C ( $n = 5$ ).

**C** Transcript levels of *Ucp1*, *Pgc1α*, *Adrb3*, *retinoblastoma 1 (Rb1)*, *zinc finger protein 423 (Zfp423)*, and *PR domain containing 16 (Prdm16)* were quantified in sWAT of WT and KO mice after 25 weeks on a HFD ( $n = 4-5$ ).

**D** Transcript levels of *Pgc1α-1b* and *Pgc1α-1a* isoforms in sWAT of WT and KO 8-week-old females maintained at 24°C (RT) or housed at 4°C for 24 h ( $n = 5$ ).

**E** Western blot for RCAN1 in various skeletal muscle groups. Each lane was loaded with 20 μg of total protein from *plantaris (PL)*, *soleus (SOL)*, *extensor digitorum longus (EDL)*, *tibialis anterior (TA)*, *red gastrocnemius (RG)*, *white gastrocnemius (WG)*, *white vastus lateralis (WV)*, *heart ventricle (HT)*, *atria*, *diaphragm (Dia)*, and *tongue (Tong)*. The lane containing brain extract was loaded with 10 μg of protein. Antibody specificity was validated by running 20 μg of protein from the heart of an *Rcan1-KO* animal (HT-KO). The asterisks \* indicate the location of putative proteolytic fragments of RCAN1.1.

**F** Transcript levels of *Sln* in skeletal muscle (tibialis anterior) of 8- to 10-week-old WT and KO mice housed at RT ( $n = 4-5$  each gender).

**G** Transcript levels of *Sln* in skeletal muscle (tibialis anterior) of 8- to 10-week-old male WT and KO animals housed at RT ( $n = 5$ ).

**H** Representative Western blot showing SLN protein in soleus muscle of 8- to 10-week-old WT and KO animals housed at RT. GAPDH was used as a loading control.

**I** Alignment of the genomic region 1.5-Kb upstream of the mammalian *Sln* gene using the ECR Browser (<http://ecrbrowser.dcode.org/>). Human was used as the reference genome. The location of conserved NFAT binding sites is indicated by blue diamonds and CREB sites by yellow. Sites were conserved across all mammalian species available in the database except opossum. Mouse, rat, and dog are provided as representative examples. The structure of the *Sln-Luc* reporter construct is aligned below.

**J** Activity of the *Sln-Luc* reporter in C2C12 myoblasts transiently transfected with an empty control vector or ones expressing constitutively active calcineurin (*CnA\**) and *Rcan1*. Luciferase activity was normalized to beta-galactosidase activity from a co-transfected vector ( $n = 3$ , assayed in duplicate).

Data information: Transcript levels were normalized to 18S. All values shown are mean ± SD. \* $P < 0.05$ ; \*\* $P < 0.01$  (two-way ANOVA with multiple comparisons in B, D, F, and J; unpaired Student's *t*-test in C and G).

transcripts by differential promoter usage and splicing [34,35]. Upstream of the classical transcript start site, *Pgc1α-1a*, there is an alternative *Pgc1α-1b* promoter under the control of the cAMP responsive CRE-binding protein (CREB). Cold activation of *Pgc1α*

expression in BAT is specific for the *Pgc1α-1b* transcript [36]. In skeletal muscle, calcineurin-regulated CRTCs have been found to coactivate CREB to drive *Pgc1α* expression [37]. Therefore, we postulated that the increase in *Pgc1α* transcript levels in the *Rcan1-KO*



mice following cold exposure would be specific for the *Pgc1 $\alpha$ -1b* isoform. *Pgc1 $\alpha$ -1b* transcript levels were below the level of detection in animals of either genotype housed at RT. After 24 h at 4°C, *Pgc1 $\alpha$ -1b* transcripts were significantly higher in the sWAT of the *KO* compared to *WT* (Fig 5D). *Pgc1 $\alpha$ -1a* was expressed in both genotypes housed at RT and was not cold-induced. These data indicate that RCAN1 suppression of *Pgc1 $\alpha$*  expression is specific for the *Pgc1 $\alpha$ -1b* transcript during cold adaptation of sWAT.

#### Loss of *Rcan1* has minimal impact on cold activation of BAT

Under basal conditions, transcript levels for *Ucp1*, *Pgc1 $\alpha$* , and *Adrb3* were not elevated in BAT of *KO* animals compared to *WT* (Fig EV4A). Similarly, cold induction of *Ucp1* and the *Pgc1 $\alpha$ -1b* isoform in BAT was of the same magnitude in *WT* and *KO* animals (Fig EV4B). Consistent with this, UCP1 protein levels in BAT were similar in *WT* and *KO* (Fig EV4C) as was the ability to maintain body temperature following a shift to 4°C (Fig EV4D). We found no genotype differences in the rates of lipolysis in BAT and gWAT, either under basal conditions or following adrenergic stimulation (Fig EV4E). However, in sWAT, the basal rate of lipolysis was significantly higher in the *KO* compared to *WT*. Following adrenergic stimulation, fold activation was much lower in the *KO* compared to the *WT* response, although the maximal stimulated rates were similar. Taken together, these data suggest that RCAN1 plays a unique role in adipose tissue stores capable of undergoing white-to-brown conversion, acting to both suppress basal rates of lipolysis and limit adrenergic activation of *Ucp1* expression during cold-induced beiging. Remarkably, loss of RCAN1 appears to have minimal impact on these processes in canonical WAT and BAT.

#### Expression of sarcolipin is increased in striated muscle of *Rcan1*-*KO* mice

The preceding data demonstrate that mice deficient for *Rcan1* have an increased adipocyte-autonomous capacity for cold and diet-induced beiging of sWAT. However, this is not likely sufficient to account for the elevated whole-body metabolic rate of young *Rcan1*-*KO* mice housed at RT (Fig 3), because these mice show no evidence of increased UCP1 compared to *WT*. In humans, adipose tissue is estimated to contribute < 1% of REE [3], whereas striated muscle contributes as much as 30%. As much as 50% of the ATP consumed by skeletal muscle in animals at rest is expended by SERCA to cycle  $\text{Ca}^{2+}$  ions [38]. RCAN1 is abundant in striated muscle [10], and forced expression in skeletal muscle can prevent formation of highly oxidative type I fibers [39]. Protein levels of RCAN1.1 were similar across a variety of skeletal muscle groups, whereas RCAN1.4 levels varied depending on the fiber-type composition of the muscle, with higher levels found in more highly oxidative muscles such as the soleus and plantaris (Fig 5E). Metachromatic staining for muscle fiber-type composition [40] (Fig EV5A) and myosin heavy chain resolution [41] (Fig EV5B) showed that the skeletal muscle of the *Rcan1* *KO* animal had not shifted toward a more oxidative fiber-type composition. If anything, there appeared to be a reduction in highly oxidative type I fibers. Thus, a shift in fiber-type composition could not explain the elevated metabolic rate. AKT phosphorylation following an insulin injection was similar in the skeletal muscle of both genotypes

(Fig EV5C), indicating a similar ability to respond to insulin, consistent with the similarity in the shapes of the ITT responses seen in Fig 2H.

Given the recent studies identifying SLN as a key determinant of basal metabolic rate and muscle-based thermogenesis [5,7], we asked whether a change in SLN levels in skeletal muscle could contribute to the elevated whole-body metabolic rate of *Rcan1*-*KO* mice. Indeed, *Slm* transcript levels were higher in the skeletal muscle of *Rcan1*-*KO* mice compared to in *WT* mice housed at 24°C (Fig 5F). In contrast to *Pgc1 $\alpha$*  and *Ucp1* in sWAT, there was no significant difference between males and females with regard to *Slm* transcript levels. Western blot analysis confirmed a corresponding increase in SLN protein levels in skeletal muscle of the *KO* mice (Fig 5G). *Slm* transcript levels were likewise elevated in the *KO* heart, another striated muscle where *Slm* is expressed (Fig 5H).

#### The *Slm* promoter responds to calcineurin

In mouse, *Slm* is preferentially expressed in muscle groups rich in oxidative fibers [42]. However, fiber-type analysis indicated that skeletal muscle in the *KO* was not more oxidative (Fig EV5A and B). Thus, the increase in SLN levels was not due to a shift in fiber-type content. Little is known regarding the transcriptional controls that mediate *Slm* expression. The ECR Browser (<http://ecrbrowser.ode.org/>) indicated two clusters of NFAT- and CREB-binding sites conserved across all available mammalian genomes (excluding opossum) (Fig 5H). To test whether this genomic region is calcineurin-responsive, the 1.5-Kb fragment was cloned upstream of a luciferase reporter (Fig 5H) and used in transient transfections of C2C12 myoblasts. Co-transfection with a plasmid encoding a constitutively active form of calcineurin (CnA\*) increased reporter activity. Co-transfection with a vector expressing *Rcan1* blocked activation of the reporter by CnA\* (Fig 5I). Taken together, these data suggest that a calcineurin-dependent increase in expression of *Slm* in the skeletal muscle of *Rcan1*-*KO* mice contributes to the elevated REE of these animals.

#### Liver and adipose tissue expression of *Rcan1* correlates with measures of metabolic syndrome

Using a publicly available data set designed to identify associations between gene expression levels in target tissues and metabolic traits in a diverse population of more than 100 unique inbred mouse strains [43], we plotted *Rcan1* gene expression in liver and adipose tissue as a function of HOMA-IR (homeostatic model of assessment of insulin resistance) after 8 weeks on a high-fat/high-sugar diet (32% kcal from fat and 25% kcal from sucrose). There was a positive correlation between *Rcan1* transcript levels and HOMA-IR index in both liver and white adipose tissue (Fig 6A). For liver, *Rcan1* ranked as the strongest positive correlation with HOMA-IR in the data set of over 22,000 microarray probesets. In adipose tissue, *Rcan1* ranked in the top 4% strongest correlations. Surprisingly, a similar analysis showed no association between *Rcan1* transcript levels in skeletal muscle and HOMA-IR (Fig EV5D). It may be relevant to note that RCAN1.1 and RCAN1.4 protein levels increased in both white adipose tissue and liver following 8 weeks on HFD (Fig EV5E). In contrast, RCAN1 protein levels did not change in skeletal muscle in response to either 8 weeks of HFD or short-term

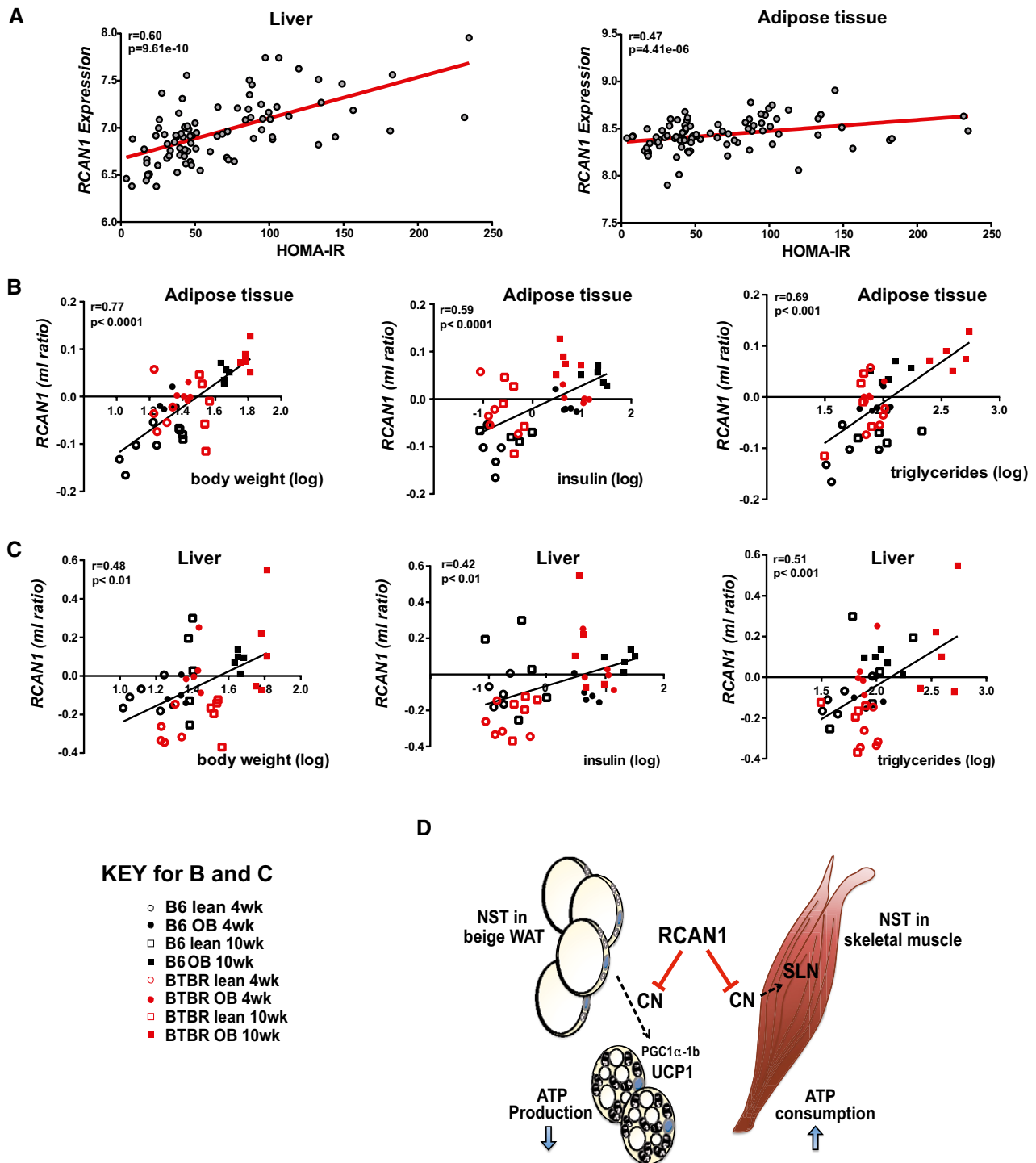


**Figure 6.** *Rcan1* expression is positively correlated with indices of metabolic syndrome.

- A** Correlation of *Rcan1* expression in liver and gonadal adipose tissue with HOMA-IR, using male mice from over 100 strains from the hybrid mouse diversity panel. Regression line (red),  $r$  = biweight midcorrelation,  $P$  =  $P$ -value.
- B, C** Correlation of *Rcan1* expression in gonadal adipose tissue and liver with body weight, plasma insulin, and plasma triglycerides, in a data set comparing backgrounds susceptible (BTBR background) or resistant (C57BL/6 background) to diabetes when carrying the *leptin<sup>ob/ob</sup>* (*ob*) mutation. Measures are reported as the ratio of the mean  $\log_{10}$  intensity (ml ratio). Regression line (black),  $r$  = linear regression,  $P$  =  $P$ -value.
- D** Model for RCAN1 suppressive control over two prominent mechanisms of mammalian non-shivering thermogenesis (NST): one in white adipose tissue, where uncoupling of the mitochondrial membrane potential by UCP1 increases heat generation at the expense of ATP production; the other in skeletal muscle, where SLN increases ATP consumption by SERCA. In adipose tissue, RCAN1 suppresses the conversion of white adipocytes to UCP1-positive, beige adipocytes by acting as a brake on calcineurin (CN)-dependent activation of *Pgc1 $\alpha$ -1b* expression, thereby blunting downstream activation of *Ucp1* expression. In skeletal muscle, RCAN1 suppresses CN-dependent expression of *Slh* directly. Loss of these repressive functions underlies the elevated metabolic rate and lean phenotype of the *Rcan1*-KO animals.

cold exposure (Fig EV5F). Thus, only tissues with a positive association between *Rcan1* transcript levels and HOMA-IR showed increased protein levels on a HFD.

Using a second data set profiling gene expression in tissues from lean and obese mouse strains that are resistant or susceptible to diabetes [44], we also found positive correlations for *Rcan1* expression in liver and adipose tissue with body weight, triglycerides, and insulin (Fig 6B and C). Taken together, these data identify the *Rcan1* gene as a gene highly correlated with metabolic syndrome, consistent with our studies of the *Rcan1*-KO mice.

## Discussion

Obesity has been estimated to reduce life expectancy by as much as 6–20 years [1,45] and is associated with an increased risk for type 2 diabetes, cardiovascular disease, and cancer. On a global level, the causes driving this epidemic in obesity are multifactorial, involving factors such as socioeconomic pressures, education, and nutritional content. On an individual level, the underlying cause lies in an imbalance between calories consumed and calories expended. However, control over this deceptively simplistic equation involves a complex network of gene–environment interactions that feed back to establish homeostatic control. Mammals evolved under the selective pressures of food limitation and environmental exposure, developing mechanisms for both long-term storage of calories and their expenditure for functions such as thermogenesis when needed. Although UCP1 and SLN act through distinct mechanisms, levels of both proteins increase in their respective tissues under prolonged exposure to cold, leading to a long-term, adaptive increase in thermogenic potential. The ability to adjust thermogenic capacity to environmental conditions is critical as it guards against unnecessary expenditure of limited energy resources when thermogenesis is not needed. Here, we provide evidence that the *Rcan1* gene acts as a centralized brake on both of these adaptive, thermogenic responses, providing systemic control over energy resources.

Although *Ucp1*-KO mice are acutely sensitive to cold temperatures, they can gradually adapt to 4°C through activation of compensatory thermogenic mechanisms [46,47], such as increasing SLN in skeletal muscle [8,48]. Conversely, *Sln*-KO animals adapt through increased expression of *Ucp1* and enhanced browning of WAT [8]. Thus, although expression of both *Ucp1* and *Sln* increases in response to cold exposure, there are systemic regulatory mechanisms that feed back to establish the appropriate balance between these two thermogenic mechanisms. In the absence of *Rcan1*, the “set-point” of this balance appears to have been raised, as both UCP1 and SLN levels are elevated in the *Rcan1*-KO, suggesting that in *WT* animals, *Rcan1* functions to limit the magnitude to which each of these thermogenic processes are activated in its respective tissue (Fig 6D).

### Rcan1 limits activation of *Pgc1α* and *Ucp1* during beiging

Here, we demonstrate that loss of *Rcan1* does not alter the ability of preadipocytes to differentiate; rather, it alters the capacity of those adipocytes to respond to adrenergic signals that promote beiging. This was most pronounced in sWAT of the *KO* mice where cold induction of *Pgc1α* and *Ucp1* expression was significantly higher

than in *WT* (Fig 5). In humans, the capacity for UCP1-dependent thermogenesis is inversely associated with insulin resistance, diabetes, and obesity [49,50]. It is relevant to note that the molecular signature of UCP1-positive adipocytes in humans more closely resembles beige adipocytes than classical BAT regardless of their location in the body [51]. Therefore, the increased beiging response displayed by *Rcan1*-KO mice may be particularly applicable to control of UCP1-dependent thermogenesis in humans.

*Pgc1α* is both required [52] and sufficient to promote *Ucp1* expression [33]. Enhanced, cold activation of *Pgc1α* expression in *Rcan1*-KO mice was specific for the alternative *Pgc1α-1b* isoform, whose expression in skeletal muscle is dependent on calcineurin-activated CRTCs [34,37]. Taken together, our results are consistent with a model in which RCAN1 acts to suppress calcineurin-/CRTC-/CREB-dependent expression of *Pgc1α-1b*, thereby suppressing adaptive increases in *Ucp1* expression during the beiging response. Relevant to our studies, a recent paper provides evidence for binding of CRTC3 directly to the *Ucp1* locus [53], potentially placing *Ucp1* under control of RCAN/calcineurin both in parallel with and downstream of *Pgc1α-1b*.

### Rcan1 suppresses *Sln* expression in skeletal muscle

Both *in vitro* and *in vivo* studies suggest that *Sln* is under the control of calcineurin (Fig 5). Based on the sequence alignment of the proximal promoter, there are evolutionarily conserved binding sites for NFAT and CREB, either of which is capable of mediating calcineurin-dependent control. Whether these signaling pathways act in concert or individually to influence *Sln* expression is yet to be determined. Skeletal muscle-specific deletion of SIK1, a suppressor of CRTC-mediated transcription, improves insulin sensitivity and glucose disposal in mice on a HFD [54], highlighting the relevance of CRTC pathway to skeletal muscle-mediated glucose control.

In rodents, *Sln* is preferentially expressed in oxidative fibers [42], the muscle fiber-type associated with higher calcineurin activity [55]. In larger mammals, including humans, SLN levels are an order of magnitude higher than in rodents and not restricted to slow fiber-type muscles [42,56]. Thus, SLN may contribute to a larger share of NST in humans than in mice. Similar to the *Rcan1*-KO mice, transgenic mice with skeletal muscle-specific overexpression of *Sln* have a higher whole-body metabolic rate, consume more calories, gain less weight on a HFD, and have lower glucose levels following a fast [57], demonstrating that increased *Sln* expression could be sufficient to cause this array of phenotypes in the *Rcan1*-KO. However, calcineurin signaling is a central mediator of skeletal muscle metabolic adaptation [58]. It would therefore be naive to assume that elevated SLN content is the only metabolically relevant change in the skeletal muscle of the *Rcan1*-KO animals.

### Rcan1 acts in multiple tissues

Calcineurin and its regulator RCAN1 are involved in many physiological processes capable of impacting metabolism. In the pancreas, expression of a number of genes important for β-cell proliferation is under the control of NFAT [59]. We previously showed that systemic overexpression of *Rcan1.1* inhibits glucose-stimulated insulin secretion from β-cells [26,27] and influences vesicle

recycling [60,61]. Furthermore, overexpression of *Rcan1.1* in acinar cells blocks pancreatic growth [62]. It was therefore surprising to find that plasma insulin levels in young *Rcan1-KO* mice were similar to those of *WT* on a normal chow diet, and increased similarly on the HFD, although phenotypic differences did manifest with aging (Fig EV2B). Calcineurin signaling is important in immune responses, and indeed, *Rcan1* is present in a variety of cell types of both the innate and adaptive immune systems [63–66]. RCAN1 can suppress NF- $\kappa$ B activation [67], and *Rcan1-KO* mice show enhanced inflammatory responses [68,69]. Thus, the reduction in inflammatory markers in the gWAT of the *KO* mice on HFD is likely secondary to the lean phenotype rather than due to suppression of an immune response in the *KO*. Along these same lines, endothelial cell dysfunction is a prominent feature of diabetes [70], whereas RCAN1 promotes endothelial barrier integrity [71]; thus, loss of *Rcan1* in endothelial cells is not likely the driving mechanism behind the lean phenotype in our studies.

In young animals, the most prominent difference comparing *KO* to *WT* was the elevation in whole-body metabolic rate (Fig 4). As discussed earlier, the increase in SLN levels, observed in young mice housed at RT and fed NC, could be sufficient to explain this phenotype. In contrast, differences stemming from the enhanced beiging response might only become manifest following an initiating challenge, such as cold exposure or HFD feeding. It is important to note that all of the animals used in our studies were raised under normal vivarium temperatures (~23°C) rather than thermoneutral conditions. Therefore, based on the studies presented here, it is not possible to know whether the elevated metabolic rate observed in young *Rcan1-KO* mice (Fig 3) is an inherent developmental phenotype or already reflects an enhanced adaptation to the environment.

Across the genome, *Rcan1* expression in liver has the strongest positive correlation with markers of worsening metabolism and ranks within the top 4% of positive correlations in WAT [43]. The positive correlation of *Rcan1* expression in WAT with HOMA-IR, body weight, triglycerides, and insulin levels (Fig 6B and F–H), combined with our evidence that loss of *Rcan1* reduces fat storage and improves metabolic function, supports a model in which *Rcan1* acts to impair metabolism, rather being expressed downstream of metabolic change. Surprisingly, no correlation was found for *Rcan1* expression in skeletal muscle (Fig EV5D). It is interesting to note that we found no change in RCAN1 protein levels in skeletal muscle in response to either cold or HFD (Fig EV5F). This might suggest that the mechanism of action of RCAN1 relative to NST in skeletal muscle does not involve a change in RCAN1 abundance, whereas in liver and adipose tissue, it does.

A potential confounding factor when assessing RCAN1 levels is the circadian pattern of *Rcan1.4* expression reported for both skeletal muscle [72] and heart [73,74], but which may also occur in other tissues. In addition, *Rcan1* transcript levels have been shown to display seasonal changes in hibernating animals [75]. This raises the interesting possibility that daily or seasonal changes in RCAN1 levels could impact the magnitude of energy mobilization or a thermogenic response.

The fact that the strongest positive correlation between *Rcan1* expression and insulin resistance was found in liver (Fig 6A and C–E) suggests that RCAN1 is also relevant to metabolic control in this tissue. This is perhaps not surprising given

the broad tissue distribution of calcineurin and the breadth of processes dependent on calcineurin-mediated signaling. Interestingly, *Rcan2-KO* mice were recently found to be resistant to age and diet-induced obesity [76,77]. However, in contrast to the *Rcan1-KO* mice, the underlying cause in the *Rcan2-KO* mice was a reduction in food intake rather than an increase in energy expenditure, and the relevant site of action for *Rcan2* was the hypothalamus. Thus, relative to controlling metabolic balance, both RCAN family members act to conserve calories but carry out apparently distinct functions, with *Rcan2* acting in the central nervous system to promote caloric intake and *Rcan1* suppressing thermogenic expenditure of calories in peripheral tissues. Although, given RCAN1's abundance in neurons, we cannot rule out the possibility that the central nervous system also has a role in metabolic phenotype of the *Rcan1 KO* animals.

We have recently shown that loss of RCAN1 increases calcineurin-dependent mitochondrial fission both *in vitro* and *in vivo* [78]. Consistent with increased fission, we found that mitochondrial membrane potential and oxygen consumption were lower in myocytes and fibroblasts isolated from *Rcan1-KO* mice. Thus, one might predict a more fragmented mitochondrial network to reduce metabolic rate rather than increase it. However, it is intriguing to note a recent study that reports a connection between mitochondrial fission and white-to-beige conversion of human adipocytes [79]. Therefore, it is possible that, in addition to the mechanisms we have documented here, altered mitochondrial dynamics may also contribute to enhanced adaptive NST in the absence of *Rcan1*.

In conclusion, we provide evidence that *Rcan1* influences metabolism by cell-autonomous suppression of two thermogenic processes, one in adipose tissue and the other in skeletal muscle. This ability to limit energy expenditure by NST may be critical for survival when food sources are scarce but have become maladaptive in current conditions of caloric abundance. We postulate that these findings may be of particular relevance to individuals with DS, a population with increased adiposity and insulin resistance [80,81] coupled with reduced REE [82], phenotypes opposite to those observed in the *Rcan1-KO*. Given the wide range of physiological processes regulated by calcineurin, it is probable that additional points of *Rcan1*-dependent metabolic control may be identified in the future.

## Materials and Methods

### Mice

Two independently derived *Rcan1-KO* lines were used in our studies: one lacking exons 5 and 6 [83] and the other deficient for the coding regions of exon 6 and 7 [84]. Mice were maintained on a mixed 129SvJ  $\times$  C57BL/6 genetic background, homozygous for a wild-type allele of the nicotinamide nucleotide transhydrogenase locus (*Nnt*), mutation of which can dysregulate glucose homeostasis and increase weight gain on a HFD [85,86]. The two lines were indistinguishable relative to metabolic phenotype. Whenever possible, littermates from (*Het*  $\times$  *Het*) crosses were used. In addition, to increase yields, sibling mice from (*Het*  $\times$  *Het*) crosses were used to



set up (*Het* × *KO*) and (*WT* × *WT*) crosses, and to generate *KO* and *WT* animals, respectively. New breeding pairs were periodically set up from the offspring of (*Het* × *Het*) crosses. Experimental animals were age-matched and always only one generation away from the founding (*Het* × *Het*) cross. Unless otherwise noted, animals were housed at 23°C under standard vivarium conditions under a 12:12-h light:dark cycle. Animals were allowed free access to water and were fed *ad libitum* either a normal chow diet (NC), in which 4% of the caloric content derived from fat (LabDiet 5001), a high-fat diet (HFD) in which 60% of the calories derived from fat (Research diet D12492), or a 35% fat diet of similar composition produced by Specialty Feeds (WA, Australia). Food consumption and body weight were recorded weekly. For cold-induction experiments, mice were housed at 6°C under a 12:12-h light:dark cycle with free access to food and water. All animal procedures were carried out with the oversight and approval of the University's Institutional Animal Care and Use Committee and conformed to the current *Guide for the Care and Use of Laboratory Animals*, published by the National Institutes of Health. Unless otherwise noted, tissues were harvested between 10 AM and 2 PM.

### Cell lines

3T3-L1 preadipocytes (ATCC) were cultured at 37°C, 5% CO<sub>2</sub>, 21% O<sub>2</sub>, in a growth medium of Dulbecco's modified Eagle's medium with high glucose plus pyruvate, supplemented with 10% (v/v) fetal calf serum, 100 units/ml penicillin G, and 100 mg/ml streptomycin. Two days after reaching confluence (day 0), cells were treated for 2 days with growth medium plus MDI (0.5 mM methylisobutylxanthine, 1 μM dexamethasone, and 10 μg/ml insulin, all from Sigma) to induce differentiation. At day 2 differentiation, media were replaced with growth medium containing 10 μg/ml insulin for 2 days and then every 2 days thereafter with growth medium alone. Samples of media were removed prior to each change for analysis of adiponectin content by Western blot. After 10 days, cells were harvested for protein and RNA or fixed with formalin and stained with Oil Red O. ON-TARGETplus siRNAs (Dharmacon) were used to deplete RCAN1. Preadipocyte cultures were grown to confluence then transfected with a non-specific control siRNA (IDT) or siRNAs targeting RCAN1.1 (UGGAGGAGGUGGAUCUGCAUUU) and RCAN1.4 (GAUGAUGUCUUCAGCGAAAUU) using Lipofectamine<sup>®</sup>RNAiMax reagent. 48 h after transfection, differentiation was initiated using MDI. The immortalized *Ing-svf* preadipocyte cell line was derived by serial 3T3 passaging of plastic-adherent inguinal WAT SVF cells of *WT* mice [87]. PDGFR $\alpha^+$ /Lin $^-$  adipose tissue stem cells were isolated from the SVF of *WT* and *Rcan1-KO* animals by flow cytometry, then differentiated as previously described [88].

### Glucose and insulin tolerance tests

For the glucose tolerance test (GTT), mice were fasted for 16 h then gavaged with 1 g/kg body weight glucose. For insulin tolerance test (ITT), mice were fasted for 3 h then injected interperitoneally with 1 unit/kg body weight insulin. Mice had access to water *ad libitum* during this period. Blood was sampled from the tail. Serum glucose was measured using the glucose-GO assay kit (Sigma-Aldrich GAGO), and insulin was measured by ELISA (Sigma-Aldrich RAB0817).

### Fecal triglyceride and cholesterol

Feces were collected over the course of 3 days and stored at -20°C until extraction. Samples were homogenized with chloroform/methanol to extract lipids and cholesterol following standard procedures [89]. Triglycerides and cholesterol were quantified using commercially available kits (BioVision K622 and K603) according to the manufacturer's instructions. Concentrations were determined based on a standard curve and expressed as mM/mg feces. Triglyceride and cholesterol were extracted from normal and HFD chow pellets for comparison.

### Metabolic chambers and body composition

Whole-body metabolic rates were assessed using CLAMS system metabolic chambers (Columbus Instruments) in the Mouse Metabolic Phenotyping Core Facility at University of Texas Southwestern Medical Center. Mice had free access to food and water and were allowed to adapt to the metabolic cage for 24 h prior to data collection. Body composition parameters were measured by NMR in a Bruker Minispec mq10 system. Magnetic resonance imaging analysis was carried out using ITK-SNAP [90] with voxel spacing of 0.45 × 0.45 × 0.50. Visceral adipose and subcutaneous adipose tissues were manually segmented slice by slice on the basis of differences in signal intensity and location. Subcutaneous and visceral fat area was determined by total voxel area (mm<sup>3</sup>).

### Histology

Adipose tissue was isolated and fixed in 4% paraformaldehyde (PFA) and processed for H&E staining. Anti-UCP1 antibody (Fisher Scientific, PA1-24894) at a dilution of 1:500 was used on fat pads fixed overnight in 10% formalin. Prior to Oil Red O staining of liver sections, tissues were fixed in 4% PFA overnight, incubated for 12 h in 12% sucrose, then overnight in 18% sucrose overnight before being cryoembedded and sectioned by the University of Texas Southwestern Medical Center Histology Core Facility. Adipocyte size and Oil Red O staining were quantified using ImageJ software (NIH, Bethesda, MD). For fiber-type analysis, the gastrocnemius/plantaris skeletal muscle group was isolated from male animals at 12 weeks of age and embedded in a 3:1 ratio of Tissue Freezing Medium to gum tragacanth. Samples were flash-frozen and sectioned on a cryostat-microtome. Metachromatic ATPase fiber-type staining was performed using standard Brooke & Kaiser histochemistry methods with CaCl<sub>2</sub> and toluidine-blue protocol variations according to Ogilvie & Feedback as previously described [40].

### Silver-stained high-resolution glycerol gels

Total proteins including myosins were extracted from freshly frozen muscles in extraction buffer (0.3 M KCl, 0.1 M KH<sub>2</sub>PO<sub>4</sub>, 50 mM K<sub>2</sub>HPO<sub>4</sub>, 10 mM EDTA, pH 6.5) with the addition of cOmplete Protease Inhibitor Cocktail (Roche; Indianapolis, IN) as described previously [39,91]. The protein extracts were diluted 1:1 (v/v) with 60% glycerol, and 0.02 μg of protein was separated on an 8% polyacrylamide gel containing 30% glycerol. The gels were run at 4°C for 40 h at 70 V. Following electrophoresis, the gels were silver-stained with Silver Stain Plus (Bio-Rad).

**Table 1. PCR Primers.**

Gene	Symbol	Forward primer	Reverse primer
Adrenoceptor beta 3	<i>Adrb3</i>	TGC GCA CCT TAG GTC TCA TTA	AAG GCG GAG TTG GCA TAG C
Fatty acid transporter	<i>CD36</i>	GCC AAG CTA TTG CGA CAT GA	AAG GCA TTG GCT GGA AGA AC
Carnitine palmitoyltransferase I a	<i>Cpt1a</i>	GTG ACG TTG GAC GAA TCG GA	TCG GTG GCC ATG ACA TAC TC
Carnitine palmitoyltransferase I b	<i>Cpt1b</i>	TGT CAC TTC TGT CGC CAC CT	CAC CTC ATA ACG CTG GCT TC
Diacylglycerol O-acyltransferase	<i>Dgat</i>	GTG GCC TTA CTGG TTGA GTC	CTG GAT AGC TCAC AGC TTGC
Deiodinase type II	<i>Dio2</i>	CTT CCT CCT AGA TGC CTA CAA AC	CGA GGC ATA ATT GTT ACC TGA TTC
Macrophage antigen F4/80	<i>F480</i>	CTT TGG CTA TGG GCT TCC AGT C	GCA AGG AGG ACA GAG TTT ATC GTG
Facilitated glucose transporter	<i>Glut4</i>	CCC CCG ATA CCT CTA CAT CAT C	GCA TCA GAC ACA TCA GCC CAG
Glycerol-3-phosphate acyltransferase	<i>Gpat</i>	GGA ATA CAG CCT TGG CCG AT	CTC TGT GGC GTG CAG GAA TA
Monocyte chemoattractant protein-1	<i>Mcp-1</i>	GGC TCA GCC AGA TGC AGT TAAC	GCC TAC TCA TTG GGA TCA TCT TG
Pyruvate dehydrogenase acetyl-transferase	<i>Pdk4</i>	TTC ACA CCT TCA CCA CAT GC	AAA GGG CGG TTT TCT TGA TG
<i>Ppar</i> $\gamma$ coactivator 1 alpha—total	<i>Pgc1<math>\alpha</math></i>	CGG AAA TCA TAT CCA ACC AG	TGA GAA CCG CTA GCA AGT TTG
<i>Ppar</i> $\gamma$ coactivator 1 alpha—1a	<i>Pgc1<math>\alpha</math>-1a</i>	GGG ACA TGT GC AGC CAA GA	AAG AGG CTG GTC CTC ACC AA
<i>Ppar</i> $\gamma$ coactivator 1 alpha—1b	<i>Pgc1<math>\alpha</math>-1b</i>	GAC ATG GAT GTT GGG ATT GTC A	ACC AAC CAG AGC AGC ACA TTT
Peroxisome proliferator-activated gamma	<i>Ppar<math>\gamma</math>2</i>	GCA TCA GGC TTC CAC TAT GGA	AAG GCA CTT CTG AAA CCG ACA
PR domain containing 16	<i>Prdm16</i>	CTT CTC CGA GAT CCG AAA CTT C	GAT CTC AGG CCG TTT GTC CAT
Retinoblastoma 1	<i>Rb1</i>	CTG GCC TGT GCT CTT GAA GTT	CCA CGG GAA GGA CAA ATC TGT
Regulator of calcineurin 1—exon 1	<i>Rcan1.1</i>	TAG ATG GAG GAG GTG GAT CTG C	TCC TTG TCA TAT GTT CTG AAG AGG G
Regulator of calcineurin 1—exon 4	<i>Rcan1.4</i>	CCC GTG AAA AAG CAG AAT GC	TCC TTG TCA TAT GTT CCT GAA GAG GG
Stearoyl-coenzyme A desaturase	<i>Scd1</i>	GCC GAG AAG CTG GTG ATG TT	ATA GAG ATG CGC GGA ACT GT
Sarcolipin	<i>Slh</i>	GCT CCT CTT CAG GAA GTG AAG	TGG CCC CTC AGT ATT GGT AGG
Tumor necrosis factor-alpha	<i>Tnf-<math>\alpha</math></i>	GTA CCT TGT CTA CTC CCA GGT TCT CT	GTG TGG GTG AGG AGC ACG TA
Uncoupling protein 1	<i>Ucp1</i>	GCC AAA GTC CGC CTT CAG AT	TGAT TTG CCT CTG AAT GCC C
Zinc finger protein 423	<i>Zfp423</i>	CCC CCT GAT GGG AAT AAT GC	GCA ATG CGC CTG TTG GA

### Preparation of RNA and real-time PCR

RNA was extracted from tissues using either an RNeasy Mini Kit (QIAGEN) or in TRIzol (Invitrogen) using a TissueLyser (Qiagen). First-strand cDNA was synthesized using SuperScript III (Invitrogen). Real-time PCR was carried out using SYBR Green on either a Roche 480 LightCycler or a RotorGene 3000 thermocycler. Transcript levels were normalized to 18S rRNA transcript levels, and changes in expression calculated using a  $2^{-\Delta\Delta CT}$  method. All samples were run in triplicate. Primer sequences and other information for all target genes are provided in Table 1.

### Blood chemistry

Circulating levels of insulin, leptin, and adiponectin were measured by ELISA. Serum levels of nonesterified free fatty acids (FFA) were measured following a NEFA-HR (2) assay protocol (Wako Diagnostics).

### Western blot analysis

From tissue culture, total soluble protein extracts were isolated in M-PER reagent (Thermo Fisher 78505) with protease and phosphatase inhibitors (Thermo Fisher 78442). Protein extracts from skeletal muscle, heart, and liver were isolated using RIPA buffer

(150 mM NaCl, 50 mM Tris-HCl pH 7.4, 1% Triton X-100, 0.5% Na deoxycholate, 0.1% SDS, 5 mM EDTA, 2 mM EGTA) plus protease and phosphatase inhibitors in a Dounce homogenizer. Lysates were cleared by centrifugation. To extract proteins from adipose (BAT, sWAT, and gWAT), tissues were homogenized in adipose tissue lysis buffer (50 mM HEPES, 150 mM NaCl, 10% glycerol, 1% Triton X-100, pH 7.5, plus inhibitors), incubated on ice for 30 min, then centrifuged at  $18,000 \times g$  at 4°C for 20 min. The fat cake on top was discarded, and supernatant moved to a clean tube. Protein concentrations were measured using BCA (ThermoFisher 23225) and then run on standard 4–20% Tris-glycine SDS-PAGE. For detecting SLN in skeletal muscle, separate extracts were made by homogenizing in M-PER reagent with inhibitors then measuring the protein concentration of the combined soluble and insoluble lysate. 4 $\times$  SDS loading buffer (without EGTA) was added, and DNA was removed from the total protein extract by spinning through glass wool. Protein extracts were fractionated on 16% tricine-SDS-PAGE gels [92], then transferred to nitrocellulose. Polyclonal, rabbit anti-SLN antibody (Millipore ABT13, Lot 2622046) 1:1,000 was followed by goat anti-Rabbit fluorescent secondary (LI-COR, P/N 925-32211) and visualized using a LI-COR Odyssey<sup>®</sup> imaging system. Densitometry analysis of relative protein levels on Western blots was performed using Image Studio Digits (LI-COR). Other antibodies included the

**Table 2. Sources for key resources.**

Reagent or resource	Source	Identifier
<b>Antibodies</b>		
Rabbit Anti-Sarcolipin antibody	Millipore	Cat#ABT13, lot 2622046
Rabbit Anti-UCP1 antibody	Thermo Fisher	Cat#PA1-24894
Rabbit Anti-DSCR1 antibody	Sigma	Cat#D6694
Mouse Anti- $\alpha$ Tubulin antibody (B-7)	Santa Cruz	Cat#Sc-5286
Mouse Anti-Adiponectin	Thermo Fisher	Cat#MA1-054
Mouse Anti-GAPDH	Fitzgerald	Cat#10R-G109a
IRDye 800CW Goat anti-rabbit IgG	LI-COR	Cat#P/N 925-32211
IRDye 680RD Goat anti-mouse IgG	LI-COR	Cat#P/N 925-68070
<b>Chemicals, peptides, and recombinant proteins</b>		
SuperScript III First-strand Synthesis SuperMix	Thermo Fisher	Cat#18080400
TRIZol	Thermo Fisher	Cat#15596026
LightCycler FastStart Master SYBR Green I	Roche	Cat#03003230001
RNeasy Mini Kit	Qiagen	Cat#74104
FuGENE HD	Promega	Cat#E2311
Lipofectamine <sup>®</sup> RNAiMax	Thermo Fisher	Cat#13778030
M-PER Mammalian Protein Extraction Reagent	Thermo Fisher	Cat#78501
Protease & Phosphatase inhibitor cocktail	Thermo Fisher	Cat#78442
High Fat Diet (60% fat)	Research Diets	Cat#D12492
Normal Chow Diet	LabDiet	Cat#5001
<b>Critical commercial assays</b>		
Glucose (GO) Assay Kit	Sigma-Aldrich	Cat#GAGO
Mouse Ins1/Insulin-1 ELISA kit	Sigma-Aldrich	Cat#RAB0817
Mouse Leptin ELISA Kit	Sigma-Aldrich	Cat#RAB0334
Mouse Adiponectin ELISA Kit	Sigma-Aldrich	Cat#RAB1115
Triglyceride Quantification Kit	BioVision	Cat#K622
Total Cholesterol and Cholesteryl Ester Colorimetric/Fluorometric Assay Kit	BioVision	Cat#K603
Nonesterified free fatty acid assay	Wako Diagnostics	HR series NEFA-HR (2)
<b>Experimental models: cell lines</b>		
C2C12 mouse myoblasts	ATCC	CRL-1772
3T3-L1	ATCC	CL-173
<i>Ing-suf</i>	This study	
<b>Experimental models: organisms/strains</b>		
<i>Rcan1-KO</i> (129Svj):C57BL/6)	Vega et al [83]	
<i>Rcan1-KO</i> (129Svj):C57BL/6)	Porta et al [84]	
<b>Oligonucleotides</b>		
Primers for RT-qPCR	IDT	See Table 1
Forward primer for cloning <i>pSln-Luc</i> ACGCGTGCTAGCTTCTAAGCCCCATTTAGC	IDT	
Reverse primer for cloning <i>pSln-Luc</i> AAGCTTAGATCTCCGGCTGTCTGAGCTCCTGG	IDT	
siRNA targeting mouse <i>Rcan1.1</i> UGGAGGAGGUGGAUCUGCAUUU	ON-TARGETplus siRNA, Dharmacon	
siRNA targeting mouse <i>Rcan1.4</i> GAUGAUGUCUUCAGCGAAUUU	ON-TARGETplus siRNA, Dharmacon	

Table 2. (continued)

Reagent or resource	Source	Identifier
SMARTpool: ON-TARGETplus Rcan1 siRNA	Dharmacon	L-056697-01-0005
Non-targeting siRNA control Pool	Dharmacon	D-001810-10-05
<b>Recombinant DNA</b>		
<i>pSln-Luc</i> : sarcolipin luciferase reporter	This study	
<i>pCnA*-HA</i> : constitutively active calcineurin-HA-Tag	Rothermel et al [10]	
<i>pRCAN1.4-HA</i> : Rcan1.4 expression vector-HA-Tag	Rothermel et al [10]	
<b>Software and algorithms</b>		
GraphPad Prism7	GraphPad	<a href="http://www.graphpad.com/scientific-software/prism/">http://www.graphpad.com/scientific-software/prism/</a>
<b>Other</b>		
CLAMS system metabolic chambers	Columbus Instruments	<a href="http://www.touchstonediabetescenter.org/MetabolicCore/metabolic-cage.html">http://www.touchstonediabetescenter.org/MetabolicCore/metabolic-cage.html</a>
Bruker Minispec mq10—MRI	Bruker	<a href="http://www.touchstonediabetescenter.org/MetabolicCore/Bruker-NMR.html">http://www.touchstonediabetescenter.org/MetabolicCore/Bruker-NMR.html</a>
ITK-SNAP software application	Yushkevich et al [90]	
ImageJ software	NIH	<a href="https://imagej.nih.gov/ij/download.html">https://imagej.nih.gov/ij/download.html</a>

following: rabbit anti-DSCR1 (Sigma D6694, 1:2,000),  $\alpha$ -tubulin (Santa Cruz sc-5286, 1:1,000), adiponectin (Thermo Fisher MA1-054, 1:1,000), and GAPDH (Fitzgerald 10R-6109a, 1:1,000).

### Lipolysis in adipose tissue explants

These experiments measured lipolysis as previously described [93]. Modified Krebs-Henseleit buffer was gassed for 40 min with 95% O<sub>2</sub>/5% CO<sub>2</sub>. Glucose (5 mM) and fatty acid-free BSA (4%) were added to the buffer immediately before measurements. All experiments were conducted in a shaking water bath at 37°C. A sample (~30 mg) of sWAT, gWAT, or BAT was surgically removed and washed several times with saline and incubated in 500  $\mu$ l buffer with ongoing gentle shaking in the absence (basal) or presence of 1  $\mu$ M isoproterenol (a pan  $\beta$ -adrenergic agonist). The medium was collected 2 h later for determination of glycerol using a commercially available kit (Wako Chemicals, Neuss, Germany; Sigma, St. Louis, MO).

### *Sln-Luc* construct and luciferase assays

The proximal promoter from the mouse *Sln* gene was cloned into the NheI and BglII sites of the pGL3-Basic luciferase reporter vector (Promega) using forward (ACGCGTGCTAGCTTCTAAGCCCCATT-TAGC) and reverse (AAGCTTAGATCTCCGGCTGTCTGAGCTC CTGG) primers. Transfection of C2C12 myoblasts and luciferase assays were carried out as previously described [94] and normalized to a co-transfected  $\beta$ -galactosidase vector. Three independent transfections were assayed in duplicate.

### Statistical analysis

GraphPad Prism software (GraphPad Software, San Diego, CA) was used for data analysis. A normal distribution was assumed, and

variance was tested using Brown–Forsythe test. Statistical significance was tested using either a two-way ANOVA with Tukey's multiple comparisons or an unpaired Student's *t*-test as indicated in figure legends.

Sources for additional key reagents can be found in Table 2.

**Expanded View** for this article is available online.

### Acknowledgements

This work was supported by funding from the National Institutes of Health (HL072016, HL102478, 1U54HD087351, DK104789), American Heart Association (11POST7950051, 13POST16520009), Australian National Health and Medical Research Council (APP1088737), National Fund for Scientific and Technological Development in Chile (FONDECYT 11150282 and PAI 79150007), and the Diabetes Australia Research Trust (Y16G-KEAD).

### Author contributions

Conceptualization: DR, HP, DJK, and BAR; Methodology: DBG, CFJ, BWP, AJL, DRM, MJW, RKG, and MAP; Investigation: DR, HP, DBG, AMM, JB, VP, CH, CRM, DM, BWP, NUNN, MO, II, TJ, DRM, RKG, and BAR; Writing—original draft: DR, HP, DJK, and BAR; Writing—review & editing: HAS, DRM, MAP, DJK, and BAR; Funding acquisition, HAS, RKG, DJK, and BAR.

### Conflict of interest

The authors declare that they have no conflict of interest.

### References

- Bouret S, Levin BE, Ozanne SE (2014) Gene-environment interactions controlling energy and glucose homeostasis and the developmental origins of obesity. *Physiol Rev* 95: 47–82
- Harms M, Seale P (2013) Brown and beige fat: development, function and therapeutic potential. *Nat Med* 19: 1252–1263



3. Rolfe DF, Brown GC (1997) Cellular energy utilization and molecular origin of standard metabolic rate in mammals. *Physiol Rev* 77: 731–758
4. Shaikh SA, Sahoo SK, Periasamy M (2016) Phospholamban and sarcolipin: are they functionally redundant or distinct regulators of the sarco(endo)plasmic reticulum calcium ATPase? *J Mol Cell Cardiol* 91: 81–91
5. Bal NC, Maurya SK, Sopariwala DH, Sahoo SK, Gupta SC, Shaikh SA, Pant M, Rowland LA, Goonasekera SA, Molkentin JD et al (2012) Sarcolipin is a newly identified regulator of muscle-based thermogenesis in mammals. *Nat Med* 18: 1575–1579
6. Gamu D, Trinh A, Bombardier E, Tupling AR (2015) Persistence of diet-induced obesity despite access to voluntary activity in mice lacking sarcolipin. *Physiol Rep* 3: e12549
7. Maurya SK, Periasamy M (2015) Sarcolipin is a novel regulator of muscle metabolism and obesity. *Pharmacol Res* 102: 270–275
8. Rowland LA, Bal NC, Kozak LP, Periasamy M (2015) Uncoupling protein 1 and sarcolipin are required to maintain optimal thermogenesis, and loss of both systems compromises survival of mice under cold stress. *J Biol Chem* 290: 12282–12289
9. Fuentes JJ, Genescà L, Kingsbury TJ, Cunningham KW, Pérez-Riba M, Estivill X, la Luna de S (2000) DSCR1, overexpressed in Down syndrome, is an inhibitor of calcineurin-mediated signaling pathways. *Hum Mol Genet* 9: 1681–1690
10. Rothermel B, Vega RB, Yang J, Wu H, Bassel-Duby R, Williams RS (2000) A protein encoded within the Down syndrome critical region is enriched in striated muscles and inhibits calcineurin signaling. *J Biol Chem* 275: 8719–8725
11. Heisel O, Heisel R, Balshaw R, Keown P (2004) New onset diabetes mellitus in patients receiving calcineurin inhibitors: a systematic review and meta-analysis. *Am J Transplant* 4: 583–595
12. López-Vilella R, Sánchez-Lázaro IJ, Martínez-Dolz L, Almenar-Bonet L, Marqués-Sulé E, Melero-Ferrer J, Portolés-Sanz M, Rivera-Otero M, Domingo-Valero D, Montero-Argudo A (2015) Incidence of development of obesity after heart transplantation according to the calcineurin inhibitor. *Transplant Proc* 47: 127–129
13. Ramos EM, Hoffman D, Junkins HA, Maglott D, Phan L, Sherry ST, Feolo M, Hindorff LA (2013) Phenotype-genotype integrator (PheGenI): synthesizing genome-wide association study (GWAS) data with existing genomic resources. *Eur J Hum Genet* 22: 144–147
14. Yang TTC, Suk HY, Yang X, Olabisi O, Yu RYL, Durand J, Jelicks LA, Kim J-Y, Scherer PE, Wang Y et al (2006) Role of transcription factor NFAT in glucose and insulin homeostasis. *Mol Cell Biol* 26: 7372–7387
15. Soleimanpour SA, Crutchlow MF, Ferrari AM, Raum JC, Lu T, Rankin MM, Liu C, De León DD, Naji A, Kushner JA et al (2010) Calcineurin signaling regulates human islet  $\beta$ -cell survival. *J Biol Chem* 285: 40050–40059
16. Lawrence MC, Bhatt HS, Easom RA (2002) NFAT regulates insulin gene promoter activity in response to synergistic pathways induced by glucose and glucagon-like peptide-1. *Diabetes* 51: 691–698
17. Chen Y, Sampaio MS, Yang JW, Min D, Hutchinson IV (2012) Genetic polymorphisms of the transcription factor NFATc4 and development of new-onset diabetes after transplantation in Hispanic kidney transplant recipients. *Transplantation* 93: 325–330
18. Altarejos JY, Montminy M (2011) CREB and the CREC co-activators: sensors for hormonal and metabolic signals. *Nat Rev Mol Cell Biol* 12: 141–151
19. Choong E (2013) Influence of CRTCL1 polymorphisms on body mass index and fat mass in psychiatric patients and the general adult population. *JAMA Psychiatry* 70: 1011
20. Quteineh L, Bochud P-Y, Golshayan D, Crettol S, Venetz J-P, Manuel O, Kutalik Z, Treyer A, Lehmann R, Mueller NJ et al (2015) CRTCL2 polymorphism as a risk factor for the incidence of metabolic syndrome in patients with solid organ transplantation. *Pharmacogenomics* 17: 69–75
21. Song Y, Altarejos J, Goodarzi MO, Inoue H, Guo X, Berdeaux R, Kim J-H, Goode J, Igata M, Paz JC et al (2010) CRTCL3 links catecholamine signaling to energy balance. *Nature* 468: 933–939
22. Ou Z, Wang G, Li Q, Ma Z, Dai M, Zou F (2014) CRTCL3 polymorphisms were associated with the plasma level of total cholesterol and the risks of overweight and hypertriglyceridemia in a Chinese Han population. *Mol Biol Rep* 41: 125–130
23. Davies KJA, Ermak G, Rothermel BA, Pritchard M, Heitman J, Ahnn J, Henrique-Silva F, Crawford D, Canaider S, Strippoli P et al (2007) Renaming the DSCR1/Adapt78 gene family as RCAN: regulators of calcineurin. *FASEB J* 21: 3023–3028
24. Fuentes JJ, Pritchard MA, Estivill X (1997) Genomic organization, alternative splicing, and expression patterns of the DSCR1 (Down syndrome candidate region 1) gene. *Genomics* 44: 358–361
25. Yang J, Rothermel B, Vega RB, Frey N, McKinsey TA, Olson EN, Bassel-Duby R, Williams RS (2000) Independent signals control expression of the calcineurin inhibitory proteins MCIP1 and MCIP2 in striated muscles. *Circ Res* 87: E61–E68
26. Peiris H, Raghupathi R, Jessup CF, Zanin MP, Mohanasundaram D, Mackenzie KD, Chataway T, Clarke JN, Brealey J, Coates PT et al (2012) Increased expression of the glucose-responsive gene, RCAN1, causes hypoinsulinemia,  $\beta$ -cell dysfunction, and diabetes. *Endocrinology* 153: 5212–5221
27. Peiris H, Duffield MD, Fadista J, Jessup CF, Kashmir V, Genders AJ, McGee SL, Martin AM, Saiedi M, Morton N et al (2016) A syntenic cross species aneuploidy genetic screen links RCAN1 expression to  $\beta$ -cell mitochondrial dysfunction in type 2 diabetes. *PLoS Genet* 12: e1006033
28. Hancock AM, Witonsky DB, Gordon AS, Eshel G, Pritchard JK, Coop G, Di Rienzo A (2008) Adaptations to climate in candidate genes for common metabolic disorders. *PLoS Genet* 4: e32
29. Dodson MV, Hausman GJ, Guan L, Du M, Rasmussen TP, Poulos SP, Mir P, Bergen WG, Fernyhough ME, McFarland DC et al (2010) Lipid metabolism, adipocyte depot physiology and utilization of meat animals as experimental models for metabolic research. *Int J Biol Sci* 6: 691–699
30. Park J, Oh Y, Chung KC (2009) Two key genes closely implicated with the neuropathological characteristics in Down syndrome: DYRK1A and RCAN1. *BMB Rep* 42: 6–15
31. Yahia S, El-Farahaty RM, El-Hawary AK, El-Hussiny MA, Abdel-Maseih H, El-Dahtory F, El-Gilany A-H (2012) Leptin, insulin and thyroid hormones in a cohort of Egyptian obese Down syndrome children: a comparative study. *BMC Endocr Disord* 12: 22
32. Shoelson SE, Lee J, Goldfine AB (2006) Inflammation and insulin resistance. *J Clin Invest* 116: 1793–1801
33. Puigserver P, Wu Z, Park CW, Graves R, Wright M, Spiegelman BM (1998) A cold-inducible coactivator of nuclear receptors linked to adaptive thermogenesis. *Cell* 92: 829–839
34. Yoshioka T, Inagaki K, Noguchi T, Sakai M, Ogawa W, Hosooka T, Iguchi H, Watanabe E, Matsuki Y, Hiramatsu R et al (2009) Identification and characterization of an alternative promoter of the human PGC-1 $\alpha$  gene. *Biochem Biophys Res Commun* 381: 537–543

35. Martinez-Redondo V, Pettersson AT, Ruas JL (2015) The hitchhiker's guide to PGC-1 $\alpha$  isoform structure and biological functions. *Diabetologia* 58: 1969–1977
36. Chang JS, Fernand V, Zhang Y, Shin J, Jun H-J, Joshi Y, Gettys TW (2012) NT-PGC-1 $\alpha$  protein is sufficient to link  $\beta$ 3-adrenergic receptor activation to transcriptional and physiological components of adaptive thermogenesis. *J Biol Chem* 287: 9100–9111
37. Wu Z, Huang X, Feng Y, Handschin C, Feng Y, Gullicksen PS, Bare O, Labow M, Spiegelman B, Stevenson SC (2006) Transducer of regulated CREB-binding proteins (TORCs) induce PGC-1 $\alpha$  transcription and mitochondrial biogenesis in muscle cells. *Proc Natl Acad Sci USA* 103: 14379–14384
38. Smith IC, Bombardier E, Vigna C, Tupling AR (2013) ATP consumption by sarcoplasmic reticulum Ca<sup>2+</sup> pumps accounts for 40–50% of resting metabolic rate in mouse fast and slow twitch skeletal muscle. *PLoS ONE* 8: e68924
39. Oh M, Rybkin II, Copeland V, Czubyrt MP, Shelton JM, van Rooij E, Richardson JA, Hill JA, De Windt LJ, Bassel-Duby R et al (2005) Calcineurin is necessary for the maintenance but not embryonic development of slow muscle fibers. *Mol Cell Biol* 25: 6629–6638
40. Ogilvie RW, Feedback DL (1990) A metachromatic dye-ATPase method for the simultaneous identification of skeletal muscle fiber types I, IIA, IIB and IIC. *Stain Technol* 65: 231–241
41. Talmadge RJ, Roy RR (1993) Electrophoretic separation of rat skeletal muscle myosin heavy-chain isoforms. *J Appl Physiol* 75: 2337–2340
42. Babu GJ, Bhupathy P, Carnes CA, Billman GE, Periasamy M (2007) Differential expression of sarcolipin protein during muscle development and cardiac pathophysiology. *J Mol Cell Cardiol* 43: 215–222
43. Parks BW, Sallam T, Mehrabian M, Psychogios N, Hui ST, Norheim F, Castellani LW, Rau CD, Pan C, Phun J et al (2015) Genetic architecture of insulin resistance in the mouse. *Cell Metab* 21: 334–346
44. Keller MP, Choi Y, Wang P, Davis DB, Rabaglia ME, Oler AT, Stapleton DS, Argmann C, Schueler KL, Edwards S et al (2008) A gene expression network model of type 2 diabetes links cell cycle regulation in islets with diabetes susceptibility. *Genome Res* 18: 706–716
45. Peeters A, Barendregt JJ, Willekens F, Mackenbach JP, Mamun AI A, Bonneux L, NEDCOM, the Netherlands Epidemiology and Demography Compression of Morbidity Research Group (2003) Obesity in adulthood and its consequences for life expectancy: a life-table analysis. *Ann Intern Med* 138: 24–32
46. Enerbäck S, Jacobsson A, Simpson EM, Guerra C, Yamashita H, Harper ME, Kozak LP (1997) Mice lacking mitochondrial uncoupling protein are cold-sensitive but not obese. *Nature* 387: 90–94
47. Ukropec J, Anunciado RP, Ravussin Y, Hulver MW, Kozak LP (2006) UCP1-independent thermogenesis in white adipose tissue of cold-acclimated Ucp1<sup>-/-</sup> mice. *J Biol Chem* 281: 31894–31908
48. Bal NC, Maurya SK, Singh S, Wehrens XHT, Periasamy M (2016) Increased reliance on muscle-based thermogenesis upon acute minimization of brown adipose tissue function. *J Biol Chem* 291: 17247–17257
49. Betz MJ, Enerbäck S (2015) Human brown adipose tissue: what we have learned so far. *Diabetes* 64: 2352–2360
50. Cypess AM, Lehman S, Williams G, Tal I, Rodman D, Goldfine AB, Kuo FC, Palmer EL, Tseng Y-H, Doria A et al (2009) Identification and importance of brown adipose tissue in adult humans. *N Engl J Med* 360: 1509–1517
51. Lidell ME, Betz MJ, Dahlqvist Leinhard O, Heglund M, Elander L, Slawik M, Mussack T, Nilsson D, Romu T, Nuutila P et al (2013) Evidence for two types of brown adipose tissue in humans. *Nat Med* 19: 631–634
52. Lin J, Wu P-H, Tarr PT, Lindenberg KS, St-Pierre J, Zhang C-Y, Mootha VK, Jäger S, Vianna CR, Reznick RM et al (2004) Defects in adaptive energy metabolism with CNS-linked hyperactivity in PGC-1 $\alpha$  null mice. *Cell* 119: 121–135
53. Shan T, Xiong Y, Zhang P, Li Z, Jiang Q, Bi P, Yue F, Yang G, Wang Y, Liu X et al (2016) Lkb1 controls brown adipose tissue growth and thermogenesis by regulating the intracellular localization of CRTC3. *Nat Commun* 7: 1–11
54. Nixon M, Stewart-Fitzgibbon R, Fu J, Akhmedov D, Rajendran K, Mendoza-Rodriguez MG, Rivera-Molina YA, Gibson M, Berglund ED, Justice NJ et al (2016) Skeletal muscle salt inducible kinase 1 promotes insulin resistance in obesity. *Mol Metab* 5: 34–46
55. Chin ER, Olson EN, Richardson JA, Yang Q, Humphries C, Shelton JM, Wu H, Zhu W, Bassel-Duby R, Williams RS (1998) A calcineurin-dependent transcriptional pathway controls skeletal muscle fiber type. *Genes Dev* 12: 2499–2509
56. Odermatt A, Taschner PE, Scherer SW, Beatty B, Khanna VK, Cornblath DR, Chaudhry V, Yee WC, Schrank B, Karpati G et al (1997) Characterization of the gene encoding human sarcolipin (SLN), a proteolipid associated with SERCA1: absence of structural mutations in five patients with Brody disease. *Genomics* 45: 541–553
57. Maurya SK, Bal NC, Sopariwala DH, Pant M, Rowland LA, Shaikh SA, Periasamy M (2015) Sarcolipin is a key determinant of the basal metabolic rate, and its overexpression enhances energy expenditure and resistance against diet-induced obesity. *J Biol Chem* 290: 10840–10849
58. Tavi P, Westerblad H (2011) The role of *in vivo* Ca<sup>2+</sup> signals acting on Ca<sup>2+</sup>-calmodulin-dependent proteins for skeletal muscle plasticity. *J Physiol* 589: 5021–5031
59. Heit JJ, Apelqvist AA, Gu X, Winslow MM, Neilson JR, Crabtree GR, Kim SK (2006) Calcineurin/NFAT signalling regulates pancreatic beta-cell growth and function. *Nature* 443: 345–349
60. Keating DJ, Dubach D, Zanin MP, Yu Y, Martin K, Zhao Y-F, Chen C, Porta S, Arbonés ML, Mittaz L et al (2008) DSCR1/RCAN1 regulates vesicle exocytosis and fusion pore kinetics: implications for Down syndrome and Alzheimer's disease. *Hum Mol Genet* 17: 1020–1030
61. Zanin MP, Mackenzie KD, Peiris H, Pritchard MA, Keating DJ (2013) RCAN1 regulates vesicle recycling and quantal release kinetics via effects on calcineurin activity. *J Neurochem* 124: 290–299
62. Gurda GT, Crozier SJ, Ji B, Ernst SA, Logsdon CD, Rothermel BA, Williams JA (2010) Regulator of calcineurin 1 controls growth plasticity of adult pancreas. *Gastroenterology* 139: 609–619.e6
63. Valdor R, Mocholi E, Botbol Y, Guerrero-Ros I, Chandra D, Koga H, Gravekamp C, Cuervo AM, Macian F (2014) Chaperone-mediated autophagy regulates T cell responses through targeted degradation of negative regulators of T cell activation. *Nat Immunol* 15: 1046–1054
64. Bhoiwala DL, Kannabiran V, Hushmendy SF, Hahn A, Bhoiwala DL, Heuring JM, Crawford DR (2011) The calcineurin inhibitor RCAN1 is involved in cultured macrophage and *in vivo* immune response. *FEMS Immunol Med Microbiol* 61: 103–113
65. Lei Q-Q, Hu G-Q, Chen W, Yu S-X, Qi S, Du C-T, Gu J-M, Lin T-J, Yang Y-J (2016) Molecular immunology. *Mol Immunol* 77: 26–33

66. Wu Z, Li Y, MacNeil AJ, Junkins RD, Berman JN, Lin TJ (2013) Calcineurin-Rcan1 interaction contributes to stem cell factor-mediated mast cell activation. *J Immunol* 191: 5885–5894
67. Kim YS, Cho K-O, Lee HJ, Kim SY, Sato Y, Cho Y-J (2006) Down syndrome candidate region 1 increases the stability of the I $\kappa$ B $\alpha$  protein: implications for its anti-inflammatory effects. *J Biol Chem* 281: 39051–39061
68. Junkins RD, MacNeil AJ, Wu Z, McCormick C, Lin TJ (2013) Regulator of calcineurin 1 suppresses inflammation during respiratory tract infections. *J Immunol* 190: 5178–5186
69. García-Redondo AB, Esteban V, Briones AM, del Campo LSD, González-Amor M, Méndez-Barbero N, Campanero MR, Redondo JM, Salaices M (2018) Regulator of calcineurin 1 modulates vascular contractility and stiffness through the upregulation of COX-2-derived prostanoids. *Pharmacol Res* 133: 236–249
70. Avogaro A, Albiero M, Menegazzo L, de Kreutzenberg S, Fadini GP (2011) Endothelial dysfunction in diabetes: the role of reparatory mechanisms. *Diabetes Care* 34: S285–S290
71. Ballesteros-Martinez C, Méndez-Barbero N, Montalvo-Yuste A, Jensen BM, Gomez-Cardenosa A, Klitfod L, Garrido-Arandia M, Alvarez-Llamas G, Pastor-Vargas C, Vivanco F et al (2017) Endothelial regulator of calcineurin 1 promotes barrier integrity and modulates histamine-induced barrier dysfunction in anaphylaxis. *Front Immunol* 8: 1323
72. Dyar KA, Ciciliot S, Tagliazucchi GM, Pallafacchina G, Tothova J, Argentini C, Agatea L, Abraham R, Ahdesmäki M, Forcato M et al (2015) The calcineurin-NFAT pathway controls activity-dependent circadian gene expression in slow skeletal muscle. *Mol Metab* 4: 823–833
73. Sachan N, Dey A, Rotter D, Grinsfelder DB, Battiprolu PK, Sikder D, Copeland V, Oh M, Bush E, Shelton JM et al (2011) Sustained hemodynamic stress disrupts normal circadian rhythms in calcineurin-dependent signaling and protein phosphorylation in the heart. *Circ Res* 108: 437–445
74. Rotter D, Grinsfelder DB, Parra V, Pedrozo Z, Singh S, Sachan N, Rothermel BA (2014) Calcineurin and its regulator, RCAN1, confer time-of-day changes in susceptibility of the heart to ischemia/reperfusion. *J Mol Cell Cardiol* 74C: 103–111
75. Vermillion KL, Anderson KJ, Hampton M, Andrews MT (2015) Gene expression changes controlling distinct adaptations in the heart and skeletal muscle of a hibernating mammal. *Physiol Genomics* 47: 58–74
76. Ding L-C, Gong Q-Q, Li S-W, Fu X-L, Jin Y-C, Zhang J, Gao J-G, Sun X-Y (2017) Rcan2 and estradiol independently regulate body weight in female mice. *Oncotarget* 8: 48098–48109
77. Sun X-Y, Hayashi Y, Xu S, Kanou Y, Takagishi Y, Tang Y-P, Murata Y (2011) Inactivation of the Rcan2 gene in mice ameliorates the age- and diet-induced obesity by causing a reduction in food intake. *PLoS ONE* 6: e14605
78. Parra V, Altamirano F, Hernández-Fuentes CP, Tong D, Kyrchenko V, Rotter D, Pedrozo Z, Hill JA, Eisner V, Lavandero S et al (2018) Down syndrome critical region 1 gene, Rcan1, helps maintain a more fused mitochondrial network. *Circ Res* 122: e20–e33
79. Pisani DF, Barquissau V, Chambard J-C, Beuzelin D, Ghandour RA, Giroud M, Mairal A, Pagnotta S, Cinti S, Langin D et al (2018) Mitochondrial fission is associated with UCP1 activity in human brite/beige adipocytes. *Mol Metab* 7: 35–44
80. Basil JS, Santoro SL, Martin LJ, Healy KW, Chini BA, Saal HM (2016) Retrospective study of obesity in children with Down syndrome. *J Pediatr* 173: 143–148
81. Flore P, Bricout V-A, van Biesen D, Guinot M, Laporte F, Pépin J-L, Eberhard Y, Favre-Juvin A, Wuyam B, van de Vliet P et al (2008) Oxidative stress and metabolism at rest and during exercise in persons with Down syndrome. *Eur J Cardiovasc Prev Rehabil* 15: 35–42
82. Hill DL, Parks EP, Zemel BS, Shults J, Stallings VA, Stettler N (2013) Resting energy expenditure and adiposity accretion among children with Down syndrome: a 3-year prospective study. *Eur J Clin Nutr* 67: 1087–1091
83. Vega RB, Rothermel BA, Weinheimer CJ, Kovacs A, Naseem RH, Bassel-Duby R, Williams RS, Olson EN (2003) Dual roles of modulatory calcineurin-interacting protein 1 in cardiac hypertrophy. *Proc Natl Acad Sci USA* 100: 669–674
84. Porta S, Serra SA, Huch M, Valverde MA, Llorens F, Estivill X, Arbonés ML, Martí E (2007) RCAN1 (DSCR1) increases neuronal susceptibility to oxidative stress: a potential pathogenic process in neurodegeneration. *Hum Mol Genet* 16: 1039–1050
85. Nicholson A, Reifsnnyder PC, Malcolm RD, Lucas CA, MacGregor GR, Zhang W, Leiter EH (2009) Diet-induced obesity in Two C57BL/6 substrains with intact or mutant nicotinamide nucleotide transhydrogenase (Nnt) gene. *Obesity* 18: 1902–1905
86. Parker N, Vidal-Puig AJ, Azzu V, Brand MD (2009) Dysregulation of glucose homeostasis in nicotinamide nucleotide transhydrogenase knockout mice is independent of uncoupling protein 2. *Biochim Biophys Acta* 1787: 1451–1457
87. Todaro GJ, Green H (1963) Quantitative studies of the growth of mouse embryo cells in culture and their development into established lines. *J Cell Biol* 17: 299–313
88. Vishvanath L, MacPherson KA, Hepler C, Wang QA, Shao M, Spurgin SB, Wang MY, Kusminski CM, Morley TS, Gupta RK (2016) Mural preadipocytes contribute to adipocyte hyperplasia induced by high-fat-diet feeding and prolonged cold exposure in adult mice. *Cell Metab* 23: 350–359
89. Folch J, Lees M, Sloane Stanley GH (1957) A simple method for the isolation and purification of total lipides from animal tissues. *J Biol Chem* 226: 497–509
90. Yushkevich PA, Piven J, Hazlett HC, Smith RG, Ho S, Gee JC, Gerig G (2006) User-guided 3D active contour segmentation of anatomical structures: significantly improved efficiency and reliability. *NeuroImage* 31: 1116–1128
91. Agbulut O, Noirez P, Beaumont F, Butler-Browne G (2012) Myosin heavy chain isoforms in postnatal muscle development of mice. *Biol Cell* 95: 399–406
92. Schägger H (2006) Tricine-SDS-PAGE. *Nat Protoc* 1: 16–22
93. Stefanidis A, Watt MJ, Cowley MA, Oldfield BJ (2017) Prevention of the adverse effects of olanzapine on lipid metabolism with the antiepileptic zonisamide. *Neuropharmacology* 123: 55–66
94. Oh M, Dey A, Gerard RD, Hill JA, Rothermel BA (2010) The CCAAT/enhancer binding protein beta (C/EBP $\beta$ ) cooperates with NFAT to control expression of the calcineurin regulatory protein RCAN1-4. *J Biol Chem* 285: 16623–16631